A&A 561, A67 (2014)
DOI: 10.1051/0004-6361/201322409

Astronomy & Astrophysics

Accurate classification of 75 counterparts of objects detected in the 54-month Palermo *Swift*/BAT hard X-ray catalogue⋆,⋆⋆,⋆⋆⋆

P. Parisi[1], N. Masetti[2], A. F. Rojas[3], E. Jiménez-Bailón[4], V. Chavushyan[5], E. Palazzi[2], L. Bassani[2], A. Bazzano[1], A. J. Bird[6], G. Galaz[3], D. Minniti[3,7,8], L. Morelli[9,10], and P. Ubertini[1]

[1] Istituto di Astrofisica e Planetologia Spaziali (INAF), via Fosso del Cavaliere 100, Roma 00133, Italy
e-mail: pietro.parisi@iaps.inaf.it
[2] INAF – Istituto di Astrofisica Spaziale e Fisica Cosmica di Bologna, via Gobetti 101, 40129 Bologna, Italy
[3] Instituto de Astrofísica, Facultad de Física, Pontificia Universidad Católica de Chile, Casilla 306, Santiago 22, Chile
[4] Universidad Nacional Autónoma de México, Apartado Postal 70-264, 04510 México D.F., Mexico
[5] Instituto Nacional de Astrofísica, Óptica y Electrónica, Apartado Postal 51-216, 72000 Puebla, Mexico
[6] School of Physics & Astronomy, University of Southampton, Southampton, SO17 1BJ, UK
[7] Specola Vaticana, 00120 Città del Vaticano, Vatican
[8] Departamento de Ciencias Físicas, Universidad Andrés Bello, Av. República 220, 83701 Santiago, Chile
[9] Dipartimento di Fisica ed Astronomia "G.Galilei", Univeristà di Padova, vicolo dell'Osservatorio 3, 35122 Padova, Italy
[10] INAF – Osservatorio Astronomico di Padova, Vicolo dell'Osservatorio 5, 35122 Padova, Italy

Received 31 July 2013 / Accepted 6 November 2013

ABSTRACT

Through an optical campaign performed at four telescopes located in the northern and southern hemispheres, we have obtained optical spectroscopy for 75 counterparts of unclassified or poorly studied hard X-ray emitting objects detected with *Swift*/BAT and listed in the 54-month Palermo BAT catalogue. All these objects also have observations taken with the *Swift*/XRT, ROSAT, or *Chandra* satellites, which allowed us to reduce the high-energy error box and pinpoint the most likely optical counterpart(s). We found that 69 sources in our sample are active galactic nuclei (AGNs) of which, 35 are classified as type 1 (with broad and narrow emission lines), 33 are classified as type 2 (with only narrow emission lines), and one is a high-redshift quasi-stellar object; the remaining 6 objects are galactic cataclysmic variables. Of the type 1 AGNs, 32 are objects of intermediate Seyfert type (1.2–1.9) and one is narrow-line Seyfert 1 galaxy; for 29 of the 35 type 1 AGNs, we have been able to estimate the central black hole mass and the Eddington ratio. Of the type 2 AGNs, two display optical features typical of the low-ionization nuclear emission-line region class, three are classified as transition objects, one is a starburst galaxy, and two are X-ray bright, optically normal galaxies. All galaxies classified in this work are relatively nearby objects (0.006–0.213) except for one at redshift 1.137.

Key words. line: identification – instrumentation: spectrographs – methods: data analysis – techniques: spectroscopic

1. Introduction

A critically important region of the astrophysical spectrum is the hard X-ray band, from 15 keV to 200 keV; this band is being explored in detail by two satellites, INTEGRAL (Winkler et al. 2003) and *Swift* (Gehrels et al. 2004), which carry on board the high-energy instruments IBIS (Ubertini et al. 2003) and BAT (Barthelmy 2004), respectively. These spacecrafts permit the study of a variety of processes that take place in this observational window, thus providing a deeper look into the physics of hard X-ray sources.

Both instruments have detected a large number of known and new objects, discovered new classes of sources, and allowed us find and study highly absorbed objects. In particular, the nature of many sources detected above 20 keV by the two satellites is often unknown, because the sources are optically unclassified and their types are only inferred based on a few available X-ray or radio observations.

Optical follow-up observations of these objects is therefore mandatory. In particular, the optical spectra can provide not only an accurate source classification, but also fundamental parameters that together with multiwaveband studies, for example in the soft X-ray band, can determine the stellar population properties (Morelli et al. 2013), giving important information on these newly detected objects.

In this paper we continue the identification work on *Swift*/BAT sources that was started seven years ago, which has allowed the identification of about 60 objects through optical spectroscopy up to now (Landi et al. 2007; Parisi et al. 2009, 2012). In this work we focus on the optical follow-up of a number of objects with unknown classifications and/or redshifts that are reported in the 54-month *Swift*/BAT survey catalogue (Cusumano et al. 2010).

This survey covers 90% of the sky down to a flux limit of 1.1×10^{-11} erg cm^{-2} s^{-1} and 50% of the sky down to a flux

⋆ Based on observations obtained from the following observatories: Astronomical Observatory of Bologna in Loiano (Italy); Observatorio Astronómico Nacional (San Pedro Mártir, Mexico), Astronomical Observatory of Asiago (Italy), Cerro Tololo Interamerican Observatory (Chile).

⋆⋆ Tables 2 and 3 and Fig. 2 are available in electronic form at http://www.aanda.org

⋆⋆⋆ FITS files are only available at the CDS via anonymous ftp to cdsarc.u-strasbg.fr (130.79.128.5) or via http://cdsarc.u-strasbg.fr/viz-bin/qcat?J/A+A/561/A67

limit of 0.9×10^{-11} erg cm^{-2} s^{-1} in the 15–150 keV band. It lists 1256 sources, of which 57% are extragalactic, 19% are galactic, and 24% are of unknown type.

From this BAT survey, we selected a sample of 73 objects (one BAT source has three possible optical counterparts) that either had no optical identification, had not been deeply studied before, or were without published optical spectra. For all these sources, we first analysed the available X-ray data to reduce the source positional uncertainty from arcmin- to arcsec-sized radii. Within the reduced X-ray error boxes, we then identified the putative optical counterpart/s to the BAT object and then performed optical spectroscopic follow-up work. Following the method applied by Masetti et al. (2004, 2006a–d, 2008, 2009, 2010, 2012, 2013) and Parisi et al. (2009, 2012), we determined the nature of all selected objects, estimating also the central black hole mass for type 1 AGNs.

The paper is structured as follows: in Sect. 2, we provide information on the X-ray data reduction to obtain the X-ray coordinates of the likely counterparts; in Sect. 3, we describe the optical observations, the telescope employed, and provide information on the optical data reduction method used. Section 4 reports and discusses the main optical results (line fluxes, distances, Galactic and local extinction, central black hole masses, etc.). In Sect. 5, we discuss some peculiar sources, and finally in Sect. 6 we summarize the main conclusions of our work.

2. X-ray astrometry

In this section, we provide information on the search for the soft X-ray counterparts of the BAT objects. To obtain the soft X-ray coordinates, we cross-correlated the BAT positions with those in the catalogues of soft (<10 keV) X-ray sources and/or analysed archival observations. More specifically, for the present sample, we selected BAT objects that have, within their BAT error box, source detections by either ROSAT (Voges et al. 1999), *Swift*/XRT, or *Chandra*[1]. This approach was proven by Stephen et al. (2006) to be very effective in associating hard X-ray sources with a softer X-ray counterpart with a high degree of probability, which in turn drastically reduces their positional error circles to a few arcsec in radius, thus shrinking the search area by a factor of $\sim 10^4$.

For 73 of the 75 objects studied in this work, we used X-ray data acquired with the X-ray Telescope (XRT, 0.3–10 keV, Burrows et al. 2004) on board the *Swift* satellite. The XRT data were reduced using the XRTDAS standard data pipeline package (XRTPIPELINE v. 0.12.6), to produce screened event files. All data were extracted in photon-counting (PC) mode (Hill et al. 2004), only adopting the standard grade filtering (0–12 for PC) according to the XRT nomenclature. Depending on the source nature (bright or faint), we either used the longest exposure or coadded multiple observations to enhance the signal-to-noise ratio (S/N). For each BAT detection, we then analysed the 3–10 keV image of interest with XIMAGE v. 4.5.1 (single or added over more XRT pointings) to search for sources detected (at a confidence level $>3\sigma$) within the 90% *Swift*/BAT error circles; this 3–10 keV image choice ensured that we selected the hardest sources, hence the most likely counterparts to the BAT objects. We estimated the X-ray positions and relative uncertainties using the task XRTCENTROID V.0.2.9 (coordinates of the most likely counterparts are reported in Table 1). For the remaining two sources we used the positional information from the ROSAT Bright all-sky survey (Voges et al. 1999) and *Chandra* archival data, respectively (see Table 1). The *Chandra* data were reduced using the CIAO v4.5 software with the calibration database CALDB v4.5.6, provided by the *Chandra* X-ray Center and following the science threads listed on the CIAO website[2]. The resulting X-ray coordinates are all reported in Table 1 (second and third columns) together with their relative uncertainties (fourth column).

For six sources the association process has been more complicated than in the other cases: indeed, the putative counterparts of PBC J0030.5−5902, PBC J0243.9+5323, PBC J0818.5−1420, and PBC J0855.8−2855 are all outside the 90%, but inside the 99% BAT error circle; since no other object is detected inside the 90% positional uncertainty we assume these associations to be correct. For PBC J1020.5−0235 no soft X-ray source is detected in the 90% and 99% BAT error circles. We searched for possible associations in the recent 70-month BAT Catalogue (Baumgartner et al. 2013), finding two possible sources (SWIFT J1020.5−0237A and SWIFT J1020.5−0237B) with similar 14–195 keV X-ray fluxes. Taking into account their confidence levels in the energy range 3–10 keV and choosing the hardest one, it is more reasonable to associate the 54-month BAT source PBC J1020.5−0235 with SWIFT J1020.5−0237B, even though we cannot exclude a possible contribution from SWIFT J1020.5−0237A; we have therefore performed optical spectroscopy of the suggested counterpart, but have highlighted this source in Table 1 to recall that this is the only case where no straightforward X-ray association has been found. For PBC J1540.3+1415, two soft X-ray sources lie within the BAT error circle, one of which has two optical counterparts (see Table 1, where the three associations are reported as PBC J1540.3+1415-1, PBC J1540.3+1415-2, and PBC J1540.3+1415-3). In this case, the association of the real optical counterpart is not trivial (see Sect. 4.2.2).

Because we used different satellites to pinpoint the soft X-ray objects associated with the chosen BAT sources, we estimated the probability that a soft X-ray source detected by XRT, *Chandra*, or ROSAT is associated by chance with a BAT hard X-ray object. For associations of BAT sources with XRT and *Chandra* objects, we used the method of Tomsick et al. (2012); assuming an average 2–10 keV flux of 10^{-12} erg s^{-1} cm^{-2} and a mean BAT error radius of 4.5 arcmin, we estimated a probability of 2% of spurious association. For the single BAT source association with a ROSAT object we followed the method of Stephen et al. (2006), finding a probability of 1%, similar to the value found for XRT and *Chandra*. This value is also similar to that found by Stephen et al. (2006) for the associations of INTEGRAL sources and ROSAT bright objects. This means that our associations can be considered reliable, independently of which of the three soft X-ray satellites we used.

Although the error box of the ROSAT object associated with PBC J0325.6−0820 is substantially larger than that of XRT or *Chandra*, it does not affect our source association since this source is outside the Galactic plane and is associated with only one optical object in its error box.

3. Optical spectroscopy

In this section we describe the optical follow-up studies that we performed for all 75 objects. In Table 1 we list the optical coordinates of all likely counterparts as obtained from the 2MASS catalogue[3] (Skrutskie et al. 2006), except for one object whose

[1] http://cxc.harvard.edu

[2] Available at http://cxc.harvard.edu/ciao/

[3] Available at http://www.ipac.caltech.edu/2mass/

Table 1. Log of the spectroscopic observations presented in this paper (see text for details).

(1) Object	(2) RA X-ray	(3) Dec X-ray	(4) Error radius (arcsec)	(5) RA Opt (J2000)	(6) Dec Opt (J2000)	(7) Telescope+instrument	(8) λ range (Å)	(9) Disp. (Å/pix)	(10) UT date & time at mid-exposure	(11) Exposure time (s)
PBC J0000.9−0708	00 00 48.57	−07 09 13.2	3.6	00 00 48.81	−07 09 11.6	SPM 2.1 m+B&C Spc.	3450–7650	4.0	01 Nov. 2010, 06:42	2 × 1800
PBC J0030.5−5902$^{=+}$	00 30 01.29	−59 02 45.4	4.9	00 30 01.30	−59 02 45.0	CTIO 1.5 m+RC Spec.	3300–10500	5.7	24 Aug. 2009, 05:01	2 × 1800
PBC J0034.6−0424	00 34 32.93	−04 24 10.4	4.4	00 34 32.81	−04 24 12.2	SPM 2.1 m+B&C Spc.	3450–7650	4.0	11 Dec. 2009, 04:37	3 × 1800
PBC J0038.5+2336	00 38 31.83	+23 36 46.9	4.4	00 38 32.11	+23 36 48.3	SPM 2.1 m+B&C Spc.	3450–7650	4.0	18 Sep. 2009, 08:59	2 × 1800
PBC J0050.8+7648	00 51 06.18	+76 50 33.1	3.9	00 51 06.65	+76 50 35.9	*Copernicus*+AFOSC	4000–8000	4.2	10 Feb. 2011, 20:51	2 × 1800
PBC J0116.3+3102	01 16 14.47	+31 01 58.3	4	01 16 14.81	+31 02 01.8	SPM 2.1 m+B&C Spc.	3450–7650	4.0	10 Oct. 2010, 07:40	2 × 1800
PBC J0128.6−6038	01 29 06.70	−60 38 45.0	5.5	01 29 07.62	−60 38 42.4	CTIO 1.5 m+RC Spec.	3300–10500	5.7	14 Oct. 2010, 23:59	2 × 1000
PBC J0149.3−5017	01 49 22.12	−50 15 06.4	3.6	01 49 22.29	−50 15 07.4	CTIO 1.5 m+RC Spec.	3300–10500	5.7	12 Nov. 2010, 00:00	2 × 1200
PBC J0157.3+4715	01 57 11.05	+47 15 59.1	3.5	01 57 10.98	+47 15 58.9	SPM 2.1 m+B&C Spc.	3450–7650	4.0	31 Oct. 2010, 07:45	2 × 1800
PBC J0223.4+4549	02 23 32.81	+45 49 12.1	3.8	02 23 33.09	+45 49 16.2	*Cassini*+BFOSC	3500–8700	4.0	17 Nov. 2009, 18:15	1800
PBC J0238.3−6116	02 38 42.95	−61 17 20.3	3.7	02 38 43.13	−61 17 22.7	CTIO 1.5 m+RC Spec.	3300–10500	5.7	17 Nov. 2009, 05:35	2 × 1200
PBC J0243.9+5323^{+}	02 44 03.03	+53 28 28.7	4	02 44 02.96	+53 28 28.2	SPM 2.1 m+B&C Spc.	3450–7650	4.0	03 Nov. 2010, 08:11	2 × 1800
PBC J0311.9+5029	03 12 03.14	+50 29 13.0	3.6	03 12 02.91	+50 29 14.7	*Copernicus*+AFOSC	4000–8000	4.2	18 Aug. 2009, 02:44	1800
PBC J0325.6−0820^{R}	03 25 40.00	−08 14 42.5	9	03 25 39.42	−08 14 42.8	SPM 2.1 m+B&C Spc.	3450–7650	4.0	31 Oct. 2010, 09:40	2 × 1800
PBC J0359.0−3017	03 59 08.85	−30 18 13.2	4.4	03 59 08.85	−30 18 10.2	SPM 2.1 m+B&C Spc.	3450–7650	4.0	11 Dec. 2009, 06:19	1800
PBC J0429.7−6703	04 29 47.14	−67 03 20.6	3.8	04 29 47.36	−67 03 20.5	CTIO 1.5 m+RC Spec.	3300–10500	5.7	17 Oct. 2010, 05:40	2 × 1500
PBC J0440.8+2739	04 40 47.58	+27 39 47.5	3.7	04 40 47.71	+27 39 46.7	SPM 2.1 m+B&C Spc.	3450–7650	4.0	03 Nov. 2010, 10:45	2 × 1800
PBC J0459.8+2705	04 59 55.88	+27 06 01.2	4.3	04 59 56.08	+27 06 02.4	SPM 2.1 m+B&C Spc.	3450–7650	4.0	01 Feb. 2009, 04:56	2 × 1800
PBC J0515.3+1856	05 15 19.94	+18 54 52.5	4.7	05 15 19.79	+18 54 51.6	*Copernicus*+AFOSC	4000–8000	4.2	10 Feb. 2011, 22:13	2 × 1500
PBC J0532.7+1346	05 32 57.61	+13 45 08.4	4.2	05 32 57.53	+13 45 09.2	SPM 2.1 m+B&C Spc.	3450–7650	4.0	03 Nov. 2010, 12:52	2 × 1800
PBC J0535.6+4011	05 35 31.80	+40 11 15.7	3.7	05 35 32.11	+40 11 15.3	SPM 2.1 m+B&C Spc.	3450–7650	4.0	01 Feb. 2009, 06:04	2 × 1800
PBC J0543.9−4325	05 44 00.31	−43 25 27.9	4	05 44 00.11	−43 25 26.6	CTIO 1.5 m+RC Spec.	3300–10500	5.7	02 Oct. 2009, 08:29	2 × 1800
PBC J0602.5+6522	06 02 37.72	+65 22 16.0	4.6	06 02 37.94	+65 22 16.2	SPM 2.1 m+B&C Spc.	3450–7650	4.0	02 Nov. 2010, 12:09	1800
PBC J0609.4−6243	06 10 06.28	−62 43 10.9	3.7	06 10 06.52	−62 43 12.5	CTIO 1.5 m+RC Spec.	3300–10500	5.7	18 Nov. 2010, 05:57	2 × 1200
PBC J0635.0−7441	06 34 03.31	−74 46 37.6	3.7	06 34 03.55	−74 46 37.6	CTIO 1.5 m+RC Spec.	3300–10500	5.7	11 Nov. 2010, 00:00	2 × 1800
PBC J0654.5+0703	06 54 33.93	+07 03 21.4	3.6	06 54 34.18	+07 03 21.0	SPM 2.1 m+B&C Spc.	3450–7650	4.0	14 Mar. 2010, 03:10	1800
PBC J0706.7+0327	07 06 48.89	+03 24 45.0	3.6	07 06 48.93	+03 24 47.3	*Cassini*+BFOSC	3500–8700	4.0	09 Mar. 2011, 19:35	3 × 1800
PBC J0709.2−3601	07 09 14.23	−36 01 23.9	3.7	07 09 14.08	−36 01 21.7	CTIO 1.5 m+RC Spec.	3300–10500	5.7	16 Dec. 2010, 03:06	2 × 1800
PBC J0746.2−1610	07 46 16.87	−16 11 28.2	3.8	07 46 17.12	−16 11 27.7	SPM 2.1 m+B&C Spc.	3450–7650	4.0	11 Mar. 2010, 06:03	2 × 1800
PBC J0747.7−7326	07 47 38.88	−73 25 47.8	5.2	07 47 38.39	−73 25 53.3	CTIO 1.5 m+RC Spec.	3300–10500	5.7	31 Dec. 2009, 03:05	2 × 900
PBC J0749.2−8634	07 50 46.15	−86 32 09.5	3.6	07 50 47.21	−86 32 11.8	CTIO 1.5 m+RC Spec.	3300–10500	5.7	03 Dec. 2010, 06:58	2 × 1500
PBC J0803.4+0840	08 03 27.08	+08 41 51.6	3.6	08 03 27.37	+08 41 52.3	*Cassini*+BFOSC	3500–8700	4.0	17 Jan. 2011, 22:51	2 × 1800
PBC J0818.5−1420	08 18 20.24	−14 25 50.9	4.5	08 18 20.26	−14 25 52.8	*Copernicus*+AFOSC	4000–8000	4.2	10 Feb. 2011, 23:32	2 × 1800
PBC J0820.4−2801	08 20 34.05	−28 05 00.6	3.6	08 20 34.11	−28 04 58.8	SPM 2.1 m+B&C Spc.	3450–7650	4.0	13 Mar. 2010, 05:55	2 × 1800
PBC J0855.8−2855^{+}	08 55 17.59	−28 54 19.2	3.8	08 55 17.46	−28 54 21.8	SPM 2.1 m+B&C Spc.	3450–7650	4.0	11 Mar. 2010, 05:32	2 × 1800
PBC J0859.5+4456	08 59 30.41	+44 54 49.2	4.1	08 59 30.46	+44 54 50.4	*Cassini*+BFOSC	3500–8700	4.0	10 Mar. 2011, 21:20	2 × 1200
PBC J0917.2−6454	09 17 27.91	−64 56 25.1	3.7	09 17 27.16	−64 56 27.1	CTIO 1.5 m+RC Spec.	3300–10500	5.7	28 Jan. 2010, 04:09	2 × 1800
PBC J0927.8−6945	09 27 52.61	−69 44 39.1	3.8	09 27 53.09	−69 44 41.9	CTIO 1.5 m+RC Spec.	3300–10500	5.7	03 Dec. 2010, 08:06	2 × 1500
PBC J0929.6+6231	09 29 37.74	+62 32 38.1	4.5	09 29 37.91	+62 32 38.3	*Cassini*+BFOSC	3500–8700	4.0	21 Mar. 2011, 23:57	2 × 1800
PBC J0942.1+2342	09 42 04.54	+23 41 08.3	3.7	09 42 04.27	+23 41 06.6	SPM 2.1 m+B&C Spc.	3450–7650	4.0	10 Mar. 2010, 07:54	2 × 1800
PBC J0950.0+7315^{C}	09 49 46.00	+73 14 23.1	0.6	09 49 45.97	+73 14 23.3	*Cassini*+BFOSC	3500–8700	4.0	18 May 2009, 20:18	1800
PBC J1002.3+0304	10 02 07.17	+03 03 25.1	5.3	10 02 07.01	+03 03 27.7	*Cassini*+BFOSC	3500–8700	4.0	17 Jan. 2011, 00:09	2 × 1800
PBC J1017.2−0404	10 17 16.89	−04 04 53.5	3.9	10 17 16.81	−04 04 55.9	SPM 2.1 m+B&C Spc.	3450–7650	4.0	30 Jan. 2009, 08:27	2 × 1800
PBC J1020.5−0235	10 19 58.57	−02 34 36.7	3.7	10 19 58.56	−02 34 36.3	*Cassini*+BFOSC	3500–8700	4.0	09 Mar. 2011, 23:49	2 × 1800
PBC J1034.2+7301	10 34 23.14	+73 00 47.4	4	10 34 23.67	+73 00 49.9	*Cassini*+BFOSC	3500–8700	4.0	10 Mar. 2011, 23:13	1800
PBC J1113.6+7942	11 14 43.98	+79 43 37.2	4.4	11 14 43.86	+79 43 35.7	*Cassini*+BFOSC	3500–8700	4.0	20 Apr. 2010, 22:22	1800
PBC J1115.3+5425	11 15 20.31	+54 23 15.3	4.4	11 15 19.92	+54 23 16.8	SPM 2.1 m+B&C Spc.	3450–7650	4.0	30 Jan. 2009, 09:49	2 × 1800
PBC J1145.4+5858	11 45 32.78	+58 58 38.4	3.7	11 45 33.18	+58 58 40.9	SPM 2.1 m+B&C Spc.	3450–7650	4.0	11 Mar. 2010, 09:14	2 × 1800
PBC J1231.4+5759	12 31 21.95	+57 57 52.9	5.8	12 31 22.14	+57 57 52.9	*Cassini*+BFOSC	3500–8700	4.0	15 Dec. 2010, 04:12	900+1200
PBC J1240.8+2736	12 40 46.52	+27 33 52.6	4.6	12 40 46.41	+27 33 53.5	*Cassini*+BFOSC	3500–8700	4.0	22 Mar. 2011, 20:53	3 × 1800
PBC J1254.8−2655	12 54 56.30	−26 57 00.5	3.6	12 54 56.37	−26 57 02.1	SPM 2.1 m+B&C Spc.	3450–7650	4.0	12 Mar. 2010, 08:51	2 × 1800
PBC J1321.1+0858	13 20 59.29	+08 58 42.9	7.1	13 20 59.61	+08 58 42.2	SPM 2.1 m+B&C Spc.	3450–7650	4.0	11 Mar. 2010, 10:23	2 × 1800
PBC J1349.0+4443	13 49 08.34	+44 41 31.2	3.9	13 49 08.42	+44 41 29.5	*Cassini*+BFOSC	3500–8700	4.0	22 Mar. 2011, 21:09	1800
PBC J1355.5+3523	13 55 34.08	+35 20 59.8	4	13 55 33.83	+35 20 57.4	*Cassini*+BFOSC	3500–8700	4.0	01 Apr. 2011, 01:15	2 × 1800
PBC J1416.8−1158	14 16 50.08	−11 59 00.8	3.6	14 16 50.02	−11 58 57.7	SPM 2.1 m+B&C Spc.	3450–7650	4.0	12 Mar. 2010, 10:08	2 × 1800
PBC J1540.3+1415:										
PBC J1540.3+1415–1	15 40 13.24	+14 16 41.5	4.6	15 40 12.96	+14 16 43.3	SPM 2.1 m+B&C Spc.	3450–7650	4.0	15 Jun. 2012, 00:04	2 × 1800
PBC J1540.3+1415–2	15 40 13.24	+14 16 41.5	4.6	15 40 12.35	+14 16 59.3	SPM 2.1 m+B&C Spc.	3450–7650	4.0	15 Jun. 2012, 23:04	2 × 1800
PBC J1540.3+1415–3^{-}	15 40 07.94	+14 11 37.9	3.7	15 40 07.85	+14 11 37.1	SPM 2.1 m+B&C Spc.	3450–7650	4.0	11 Mar. 2010, 11:48	2 × 1800
PBC J1821.2+5957	18 21 26.79	+59 55 19.9	4.1	18 21 26.81	+59 55 20.9	*Cassini*+BFOSC	3500–8700	4.0	02 Jul. 2010, 21:44	1800
PBC J1824.2+1846	18 24 10.76	+18 46 09.0	4.2	18 24 10.83	+18 46 08.8	*Cassini*+BFOSC	3500–8700	4.0	01 Jul. 2010, 22:22	2 × 1200

Notes. Optical source coordinates are extracted from the 2MASS catalog, if not indicated otherwise, and have an accuracy better than 0.″1. Soft X-ray coordinates are extracted from XRT, *Chandra* or ROSAT observations. If not indicated otherwise, source X-ray coordinates were obtained from XRT data. $^{(=)}$ The reported optical coordinates are obtained from USN-A2.0 catalogue. $^{(C)}$ The reported X-ray coordinates are obtained from *Chandra* data. $^{(R)}$ The reported X-ray coordinates are obtained from ROSAT bright catalogue. $^{(+)}$ This source is outside BAT 90% error box, but inside the 99% one. $^{(-)}$ This source is at the edge of BAT 90% error box, inside the 99% one. The source is outside BAT 90% and 99% error box, but it is associated with a 2MASS source in the 70 month BAT catalogue.

Table 1. continued.

(1) Object	(2) RA X-ray	(3) Dec X-ray	(4) Error radius (arcsec)	(5) RA Opt (J2000)	(6) Dec Opt (J2000)	(7) Telescope+instrument	(8) λ range (Å)	(9) Disp. (Å/pix)	(10) UT date & time at mid-exposure	(11) Exposure time (s)
PBC J1826.6+3251	18 26 32.49	+32 51 27.0	3.8	18 26 32.39	+32 51 30.1	*Cassini*+BFOSC	3500–8700	4.0	01 Jul. 2010, 20:39	2 × 900
PBC J1846.0+5607	18 45 56.82	+56 10 02.5	5.2	18 45 56.89	+56 10 02.3	*Cassini*+BFOSC	3500–8700	4.0	10 Apr. 2011, 02:40	1800
PBC J1903.7+3349	19 03 48.96	+33 50 38.3	3.7	19 03 49.16	+33 50 40.8	*Cassini*+BFOSC	3500–8700	4.0	08 May 2011, 00:45	2 × 1200
PBC J1926.6+4131	19 26 30.48	+41 33 01.4	3.5	19 26 30.18	+41 33 05.3	SPM 2.1 m+B&C Spc.	3450–7650	4.0	14 Jul. 2010, 09:29	1800
PBC J2010.2+4759	20 10 17.20	+38 00 23.1	4.5	20 10 17.40	+38 00 21.5	*Cassini*+BFOSC	3500–8700	4.0	17 Nov. 2011, 17:30	2 × 1800
PBC J2035.2+2604	20 35 05.44	+26 03 29.2	3.7	20 35 05.66	+26 03 30.2	SPM 2.1 m+B&C Spc.	3450–7650	4.0	15 Jul. 2010, 08:48	2 × 1800
PBC J2116.2+2519	21 16 10.36	+25 16 58.3	3.6	21 16 10.28	+25 17 01.1	SPM 2.1 m+B&C Spc.	3450–7650	4.0	17 Jul. 2010, 10:30	1800
PBC J2123.9+3407	21 24 00.12	+34 09 12.4	4.4	21 24 00.28	+34 09 11.4	SPM 2.1 m+B&C Spc.	3450–7650	4.0	03 Nov. 2010, 04:34	2 × 1800
PBC J2124.5+0503	21 24 12.35	+05 02 43.7	3.9	21 24 12.44	+05 02 43.6	*Cassini*+BFOSC	3500–8000	4.0	23 Aug. 2011, 00:22	2 × 600
PBC J2150.7+1405	21 50 46.92	+14 06 37.0	4.6	21 50 46.76	+14 06 36.9	SPM 2.1 m+B&C Spc.	3450–7650	4.0	11 Dec. 2009, 03:31	2 × 1800
PBC J2157.4−0611	21 57 26.83	−06 10 18.4	3.6	21 57 26.78	−06 10 17.6	SPM 2.1 m+B&C Spc.	3450–7650	4.0	31 Oct. 2010, 02:58	1800
PBC J2248.8+1725	22 48 44.27	+17 27 01.4	3.6	22 48 44.31	+17 27 03.5	*Cassini*+BFOSC	3500–8000	4.0	05 Dec. 2011, 19:41	2 × 1800
PBC J2307.8+2244	23 07 49.31	+22 42 17.4	5.6	23 07 48.88	+22 42 36.8	*Cassini*+BFOSC	3500–8000	4.0	23 Aug. 2011, 02:14	2 × 1800
PBC J2307.9+4015	23 07 57.32	+40 16 37.7	3.8	23 07 57.25	+40 16 39.4	SPM 2.1 m+B&C Spc.	3450–7650	4.0	31 Oct. 2010, 05:24	2 × 1800
PBC J2343.8+0539	23 43 59.37	+05 38 22.5	4.2	23 43 59.56	+05 38 23.4	*Cassini*+BFOSC	3500–8000	4.0	27 Jul. 2010, 01:51	2 × 1800

position was extracted from the USNO-A2.0 catalogue (Monet et al. 2003).

The detailed log of all optical measurements is also reported in Table 1: we list in Col. 7 the telescope and instrument used for the observation, while the characteristics of each spectrograph are given in Cols. 8 and 9. Column 10 provides the observation date and the UT time at mid-exposure, while Col. 11 reports the exposure times and the number of spectral pointings.

The following telescopes were used for the optical spectroscopic study presented here:

- the 1.5 m at the Cerro Tololo Interamerican Observatory (CTIO), Chile;
- the 1.52 m *Cassini* Telescope of the Astronomical Observatory of Bologna, in Loiano, Italy;
- the 1.82 m *Copernicus* Telescope of the Astronomical Observatory of Asiago, Italy;
- the 2.1 m telescope of the Observatorio Astrónomico Nacional in San Pedro Martir, Mexico.

The data were reduced with the standard procedure (optimal extraction, Horne 1986) using IRAF[4]. Calibration frames (flat fields and bias) were taken on the day preceding or following the observing night. The wavelength calibration was obtained using lamp spectra acquired soon after each on-target spectroscopic acquisition. The uncertainty in the calibration was ∼0.5 Å in all cases; this was checked using the positions of background night-sky lines. Flux calibration was performed using catalogued spectrophotometric standards. Objects with more than one observation had their spectra stacked to increase the S/N.

The identification and classification approach we adopted in analysing of the optical spectra is the following: for the emission-line AGN classification, we used the criteria of Veilleux & Osterbrock (1987) and the line-ratio diagnostics of Ho et al. (1993, 1997) and Kauffmann et al. (2003) to distinguish among the Seyfert 2, low-ionization nuclear emission-line regions (LINERs; Heckman 1980), H II regions and transition objects (LINERs whose integrated spectra are diluted or contaminated by neighbouring H II regions, Ho et al. 1997). In the LINER class, some lines ([OII]$_{\lambda3723}$, [OI]$_{\lambda6300}$, and [NII]$_{\lambda6584}$) are stronger than in typical Seyfert 2 galaxies, the permitted emission-line luminosities are weak, and the emission-line widths are similar to those of type 2 AGNs. In particular, as mentioned in Ho et al. (1993), all sources with [OII] > [OIII], [NII]/H$_\alpha$ > 0.6 and [OI] > 1/3 [OIII] can be considered as LINERs. For the subclass assignation to Seyfert 1 galaxies, we used the H$_\beta$/[O III]λ5007 line flux ratio criterion presented in Winkler et al. (1992). Moreover, the criteria of Osterbrock & Pogge (1985) allowed us to distinguish between "normal" Seyfert 1 and narrow-line Seyfert 1 (NLS1): the latter are galaxies with a full width at half-maximum (FWHM) of the H$_\beta$ line lower than 2000 km s^{-1}, with permitted lines that are only slightly broader than their forbidden lines, with a [OIII]$_{\lambda5007}$/H$_\beta$ ratio <3, and finally with evident FeII and other high-ionization emission-line complexes.

We note that the spectra of all extragalactic objects are not corrected for starlight contamination (see, e.g., Ho et al. 1993, 1997), because of their limited S/N and spectral resolution. However, this does not affect our results and conclusions.

To estimate the $E(B-V)$ local optical absorption in our AGNs sample, when possible, we first dereddened the H$_\alpha$ and H$_\beta$ line fluxes by applying a correction for the Galactic absorption along the line of sight to the source. This was done using the galactic colour excess $E(B-V)_{\rm Gal}$ given by Schlegel et al. (1998) and the Galactic extinction law obtained by Cardelli et al. (1989). We then estimated the colour excess $E(B-V)_{\rm AGN}$ local to the AGN host galaxy by comparing the intrinsic line ratio and corrected that for Galactic reddening using the relation for type 2 AGNs derived from Osterbrock (1989)

$$E(B-V) = a\,\mathrm{Log}\left(\frac{\mathrm{H}_\alpha/\mathrm{H}_\beta}{(\mathrm{H}_\alpha/\mathrm{H}_\beta)_0}\right).$$

In the above relation, H$_\alpha$/H$_\beta$ is the observed Balmer decrement, $(\mathrm{H}_\alpha/\mathrm{H}_\beta)_0$ is the intrinsic one (2.86), and a is a constant with a value of 2.21. For type 1 objects, where the H$_\alpha$ is strongly blended with the forbidden narrow [NII] lines, it is difficult to obtain a reliable H$_\alpha$/H$_\beta$ estimate. In these cases, we used the H$_\gamma$/H$_\beta$ ratio, albeit H$_\gamma$ may also be blended with the [O III]$_{\lambda4363}$ line; the AGN reddening was evaluated using the same relation as described above but with the intrinsic $(\mathrm{H}_\gamma/\mathrm{H}_\beta)_0$ ratio of 0.474 and an a value of −5.17.

[4] IRAF is the Image Reduction and Analysis Facility made available to the astronomical community by the National Optical Astronomy Observatories, which are operated by AURA, Inc., under contract with the US National Science Foundation. It is available at http://iraf.noao.edu/

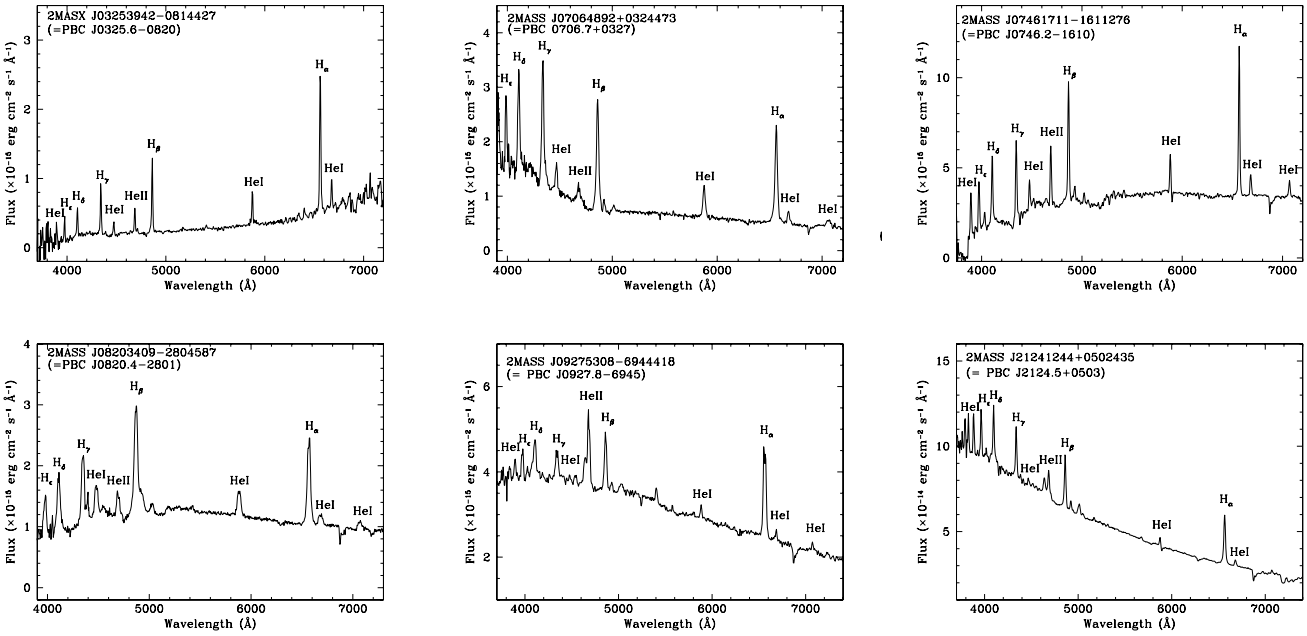

Fig. 1. Spectra (not corrected for the intervening Galactic absorption) of the optical counterparts of the six CVs belonging to the sample of BAT sources. For each spectrum the main spectral features are labelled.

To provide extra information, we also estimated the mass of the central black hole for 29 type 1 AGNs found in the sample[5]. The method used here follows the prescription of Wu et al. (2004) and Kaspi et al. (2000), where we used the H_β emission line flux, corrected for the Galactic colour excess (Schlegel et al. 1998), and the broad-line region (BLR) gas velocity ($v_{\rm FWHM}$). Using Eq. (2) of Wu et al. (2004), we estimated the BLR size, which is used with $v_{\rm FWHM}$ in Eq. (5) of Kaspi et al. (2000) to calculate the AGNs black hole mass. The results are reported in Table 6 where we also list the observed BAT X-ray luminosities in the 15–150 keV band and the Eddington ratios for each AGN considered. To calculate the luminosity distances, we considered a cosmology with $H_0 = 70\,{\rm km\,s^{-1}\,Mpc^{-1}}$, $\Omega_\Lambda = 0.7$, and $\Omega_{\rm m} = 0.3$ and used the cosmology calculator of Wright (2006).

The errors on black hole masses reported in Table 6 generally come from the emission line flux estimate that correspond to about 15%, and also from the scatter in the $R_{\rm BLR}$−$L_{\rm H_\beta}$ scaling relation (Vestergaard 2004). This implies a typical error of about 50% of the value of the black hole masses.

To derive the distance of the six cataclysmic variables (CVs) in our sample, we used the distance modulus assuming an absolute magnitude $M_V \sim +9$ and an intrinsic colour index $(V-R)_0 \sim 0$ mag (Warner 1995). Although this method basically provides an order-of-magnitude value for the distance of these Galactic sources, our past experience (Masetti et al. 2004, 2006a–d, 2008, 2009, 2010, 2012, 2013) tells us that these estimates are in general correct to within 50% of the refined value subsequently determined with more precise approaches.

4. Optical classification

In this section we discuss the optical classifications found and highlight the most interesting or peculiar objects discovered. The *R* magnitudes were all extracted from the USNO-A2.0 catalogue when not otherwise stated. Of the 75 objects studied, the majority are of extragalactic nature (69 AGNs) and only a few are of Galactic origin (6 CVs).

In the optical class, six objects in the sample had the optical type previously reported in the Véron-Cetty & Véron 13th catalogue edition (hereafter V&V13, Véron-Cetty & Véron 2010, and references therein), in the SIMBAD Astronomical Database and in Halpern (2013). Despite this, we chose to report our own data of these six sources to confirm/disclaim their classification and also to provide line flux information.

4.1. Cataclysmic variables

Six sources in our BAT sample display emission lines of the Balmer complex (up to at least H_ϵ), as well as He I and He II, consistent with $z = 0$, indicating that these objects lie within our Galaxy (see Fig. 1). The analysis of their optical features indicates that all are CVs (see Table 5). Through the equivalent widths (EW) of the H_β and He II$_{\lambda4686}$ lines we investigated their magnetic or non-magnetic nature. For PBC J0746.2−1610 and PBC J0927.8−6945 the He II$_{\lambda4686}$/H_β EW ratio is higher than 0.5, and the EW of both emission lines is larger than 10 Å, implying that both objects are magnetic CVs belonging to the intermediate polar (IP) subclass (see Warner 1995, and references therein). A tentative IP classification can also be made for PBC J0325.6−0820, PBC J0706.7+0327 and PBC J0820.4−2801 since here the He II$_{\lambda4686}$ and the H_β EW are also larger than 10 Å, although their ratio is lower than 0.5. For PBC J2124.5+0503 (classified as LMXB in Halpern 2013) the weakness of its emission lines (<10 Å) and the He II$_{\lambda4686}$/H_β ratio lower than 0.5 imply a non magnetic nature. The H_α to H_β flux ratio is lower than 2 for all the CVs found in this work, therefore we assume that the absorption along the line of sight is negligible in all cases. We also estimated their distances (see Sect. 3), assuming no Galactic extinction along the line of sight (see Table 5). All CVs that have a probably magnetic nature are located at a relatively far

[5] We were unable to estimate the mass of the central black hole of PBC J0116.3+3102, PBC J0602.5+6522, and PBC J1926.6+4131 because they all lack the H_β emission line, and of PBC J0000.9−0708, PBC J0917.2−6454, and PBC J1824.2+1846 because only the narrow component of the H_β line was observed in their spectra.

Table 4. Main results obtained from the analysis of the optical spectrum of the QSO PBC J0030.5−5902.

Object	$F_{\rm MgII}$	$F_{\rm CIII]}$	Class	z	D_L	$E(B-V)$		Optical source
					(Mpc)	Gal.	AGN	
PBC J0030.5−5902	4.67 ± 0.98 [4.9 ± 1.2]	6.82 ± 2.28 [15.6 ± 2.4]	QSO	1.137	7744.2	0.013	–	USNO-A2.0 0300−00143700

Notes. Emission line fluxes are reported both as observed and (between square brackets) corrected for the intervening Galactic absorption. Line fluxes are in units of 10^{-15} erg cm^{-2} s^{-1}. The typical error on the redshift measurement is ±0.001.

Table 5. Main optical results concerning sources identified as cataclysmic variables (see Fig. 1).

Object	H_α		H_β		He II λ4686		R	d
	EW	Flux	*EW*	Flux	*EW*	Flux	mag	(pc)
PBC J0325.6−0820	54 ± 3	30.1 ± 1.9	51 ± 3	12.9 ± 0.8	17 ± 3	4.1 ± 0.6	16.6	330
PBC J0706.7+0327	82 ± 8	48 ± 4	64 ± 5	52 ± 4	16 ± 5	14 ± 4	15.8	230
PBC J0746.2−1610	35.5 ± 2.1	128 ± 7	32.5 ± 2.4	105 ± 8	19.6 ± 2.2	55.7 ± 6.1	15.0	158
PBC J0820.4−2801	52 ± 5	55.1 ± 4.8	48 ± 8	60.1 ± 10.4	12.2 ± 1.6	14.2 ± 1.9	15.5	200
PBC J0927.8−6945	34 ± 3	83.8 ± 6.2	11 ± 2	38.7 ± 5.8	16 ± 3	60.5 ± 11.3	15.9	240
PBC J2124.5+0503	20 ± 1.9	629 ± 60	9 ± 0.8	579 ± 52	5 ± 0.9	335 ± 63	12.2	44

Notes. EWs are expressed in Å, line fluxes are in units of 10^{-15} erg cm^{-2} s^{-1}.

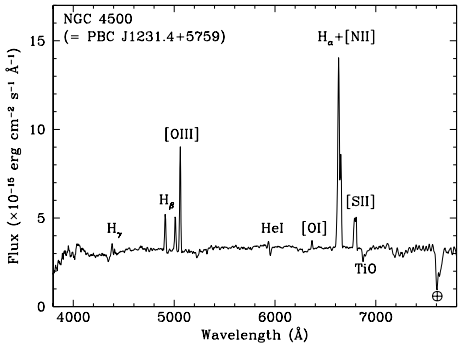

Fig. 3. Spectrum (not corrected for the intervening Galactic absorption) of the optical counterpart of the starburst galaxy belonging to the sample of BAT sources. For this spectrum the main spectral features are labelled.

distance (>150 pc), while the only non-magnetic CV is located quite close to Earth.

4.2. Extragalactic objects

The results for the extragalactic sources are reported in Tables 2 and 3, where for each source we list the H_α, H_β, and [OIII] fluxes, the classification, the estimated redshift, the luminosity distance given in Mpc, the Galactic colour excess and the colour excess local to the AGN host. In Table 4, we report information of the only quasi-stellar object (QSO) found in this sample. All the extragalactic optical spectra are displayed in Figs. 2–5.

4.2.1. Redshifts

We confirm the redshift estimates reported in SIMBAD and V&V13 for 29 AGNs. For the remaining 40 sources, the redshifts derived from our low-resolution optical spectra are published here for the first time (see Figs. 2–5). Redshift values are in the range 0.006–1.137, that is, all AGNs are located in the local Universe ($z < 0.3$) except for one source, which is at redshift 1.137.

We note that all redshifts were estimated using the [OIII] narrow emission line, and when this line was unavailable, from other forbidden narrow emission lines or absorption features.

4.2.2. Optical class

For the first time, we provide the classification of 64 sources in the sample. For the remaining five AGNs, our results agree with the classifications listed in the literature except for one object: PBC J1002.3+0304, also known as IC 0588, is classified as a Seyfert 1 in the V&V13 catalogue, but according to our analysis it is a Seyfert 1.8/1.9. PBC J2157.4−0611 was classified by Halpern (2013) in his preliminary work as a QSO, we refine this classification, stating that it is a Seyfert 1.5.

Summarizing our extragalactic results, we found that of 69 AGNs, 36 have strong redshifted broad and narrow emission-lines that are typical of Seyfert 1 galaxies, while the remaining 33 display only the strong and redshifted narrow emission-lines that are indicative of a type 2 AGN nature (for the subclass assignment see Tables 2 and 3).

Note that among broad-line AGNs, only three are pure type 1 objects, including the QSO at $z > 1$. One is an NLS1, while the remaining objects are all of intermediate type, nine belong to Seyfert 1.8–1.9, that is, they are more similar to type 2 AGNs because of the progressive disappearance of broad line regions. PBC J2035.2+2604 is the only NLS1 found; it has an optical counterpart in the USNO-A2.0 catalogue (USNO-A2.0 1125−16409384) with magnitude $R = 13.8$, a redshift of 0.05, and significant optical extinction ($E(B-V) = 0.834$ mag). NLS1 are rare among galaxies detected above 20 keV since their fraction is typically 5% of type 1 (Panessa et al. 2011) and 2% of all AGNs; this perfectly matches our findings.

Of the 33 type 2 AGNs, 22 are Seyfert 2 galaxies, 2 are LINERs, one is a starburst galaxy, 3 are transition objects, and 2 are X-ray bright, optically normal galaxies (XBONG, Comastri et al. 2002). PBC J0747.7−7326 and PBC J1321.1+0858 are classified as LINERs. The first object is a pure LINER, according to Ho et al. (1997); the second source is a less clear case

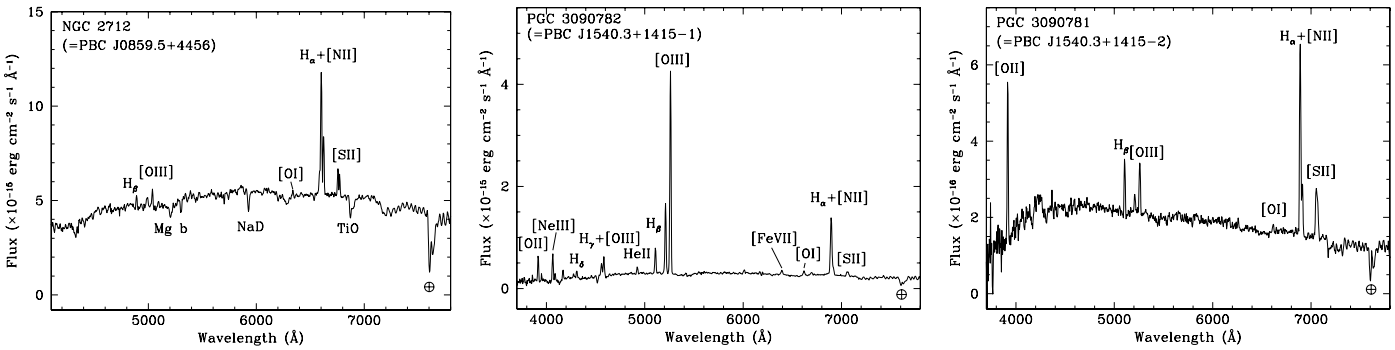

Fig. 4. Spectra (not corrected for the intervening Galactic absorption) of the optical counterparts of the three transition objects belonging to the sample of BAT sources. For each spectrum the main spectral features are labelled.

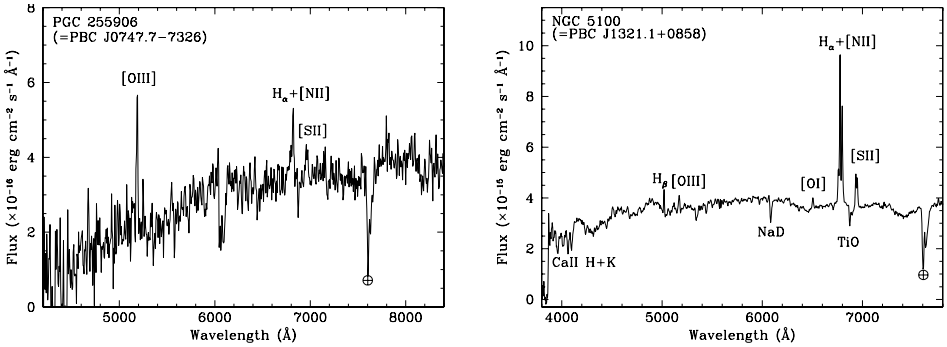

Fig. 5. Spectra (not corrected for the intervening Galactic absorption) of the optical counterparts of the two LINERs belonging to the sample of BAT sources. For each spectrum the main spectral features are labelled.

since in the Kauffmann et al. (2003) diagram it is placed in the LINERs region, but its nature is ambiguous according to the Ho et al. (1997) diagrams. We decided to classify this source as a LINER because it has some features typical of this class. Clear detection of both these objects at high energies points to an AGN (and not a burst of star formation) as the source that excites the ionized gas in these galaxies.

PBC J1231.4+5759 is classified as a starburst galaxy. In the diagrams of Ho et al. (1997) it is placed in the left part with a low [O III]/H_β ratio and a very low value [N II]/H_α ratio. It is a blue compact galaxy also known as NGC 4500. The source is characterized by intense far-infrared and UV emission typical of a recent burst of star formation. The soft X-ray counterpart of this BAT source is quite absorbed, which suggests that a low-luminosity AGN maybe hidden behind the strong signature of the starburst emission.

PBC J0859.5+4457, PBC J1540.3+1415-1 and PBC J1540.3+1415-2 are transition objects. These sources are likely LINERs whose integrated spectra are diluted or contaminated by neighbouring H II regions. Recent radio and mostly X-ray observations have suggested that these objects probably harbour low-luminosity AGNs (Ho 2008); they could represent a late stage of AGN activity when the accretion rate is lower than at the Seyfert stage. The detection of two such objects among BAT sources furthermore supports the assumption that there are low-luminosity AGN in transition galaxies. PBC J1540.3+1415-1 and PBC J1540.3+1415-2 have about the same redshift (∼0.05) and are probably in interaction; only PBC J1540.3+1415-1 has some associated radio emission, which makes it a more likely counterpart for the BAT source. We recall that the other candidate counterpart for the same BAT source is PBC J1540.3+1415-3, which is a Seyfert 1.2 at a redshift of 0.12 that displays strong radio emission (see the following section). Using the statistical method of Tomsick et al. (2012), we estimated the probability for each of these three sources to be contained by chance within the BAT hard X-ray error box and found that PBC J1540.3+1415-1 and PBC J1540.3+1415-2 have a probability of ∼0.14, with a 2–10 keV flux of 0.1×10^{-12} erg s^{-1} cm^{-2} (power law with $\Gamma = 1.8$), while PBC J1540.3+1415-3 has a probability lower than 0.02, with a 2–10 keV flux of 1.4×10^{-12} erg s^{-1} cm^{-2} (power law with $\Gamma = 1.8$), which makes it the most likely soft X-ray counterpart. On the other hand, an analysis of the XRT image at energies above 3 keV suggests that the X-ray source associated with optical objects PBC J1540.3+1415-1 and PBC J1540.3+1415-2 is the harder of the two objects detected inside the BAT positional uncertainty and is also the only one still visible above 6 keV. PBC J1540.3+1415 is clearly a complicated object that deserves more detailed studies, possibly in multiwavebands if one aims at understanding which source is responsible for the hard X-ray emission and ultimately the real nature of the BAT object.

Finally, PBC J1034.2+7301 and PBC J1355.5+3523 are both classified as XBONGs, which are X-ray bright galactic nuclei without emission lines in their optical spectra. While the presence of weak H_α and [O III] emission lines in the first source makes it more similar to a Seyfert 2, the second shows no evidence of emission lines in its optical spectrum. From a quick analysis of their X-ray spectra, both objects seem to be absorbed in X-rays with column densities above 10^{22} cm^{-2}, which suggests that they may be AGNs whose obscuration covers almost 4π of the nuclear source (see Malizia et al. 2012, for details). Additional investigation in X-rays, but also in other wavebands, can help in clarifying the nature of both sources.

5. Additional comments

We note that a number of AGNs in our sample display evidence of interaction or clustering: they either belong to a small group of objects (such as a galaxy pair or triple or a compact group) or are being disturbed by nearby galaxies. In

Table 6. Broad-line region gas velocities, central black-hole masses and apparent Eddington ratios for 29 broad-line AGNs.

Object	v_{BLR} (km s^{-1})	M_{BH} (10^7 $M_\odot$)	$L_{15-150\,keV}$ $\times 10^{43}$ erg s^{-1}	L_{15-150}/L_{Edd}
PBC J0050.8+7648	3800	7.6	43	0.04
PBC J0149.3−5017	4975	12	1.7	0.001
PBC J0157.3+4715	2600	3.2	4.8	0.01
PBC J0311.9+5029	4370	9.4	5.9	0.005
PBC J0429.7−6703	3840	7.1	4.6	0.005
PBC J0440.8+2739	3300	5.3	2.8	0.004
PBC J0532.7+1346	2000	1.9	1.1	<0.005
PBC J0535.6+4011	1600	1.2	0.7	0.004
PBC J0543.9−4325	1000	0.5	2.2	0.4
PBC J0609.4−6243	2900	4.1	31	0.06
PBC J0635.0−7441	3800	7.6	15	0.02
PBC J0654.5+0703	1700	1.5	0.9	0.005
PBC J0749.2−8634	5500	15	14	0.008
PBC J0803.4+0840	860	0.4	4.3	0.09
PBC J0818.5−1420	9400	43	21	0.004
PBC J0942.1+2342	4000	7.7	0.8	~0.001
PBC J1002.3+0304	750	0.3	0.9	0.02
PBC J1020.5−0235	11900	69	5.7	~0.001
PBC J1254.8−2655	4460	9.7	10	0.008
PBC J1349.0+4443	14500	10	9.1	0.007
PBC J1416.8−1158	12400	58	32	0.004
PBC J1540.3+1415-3	4500	9.9	35	0.03
PBC J1846.0+5607	2800	3.6	11	0.02
PBC J2035.2+2604	1600	1.2	7.4	0.05
PBC J2116.2+2519	11700	69	28	0.003
PBC J2123.9+3407	2500	3	17	0.05
PBC J2157.4−0611	3000	6.2	52	0.07
PBC J2248.8+1725	1000	0.5	15	0.2
PBC J2307.9+4015	5300	14	12	0.007

Notes. The final uncertainties on the black hole mass estimates are about 50% of their values. The velocities were determined using H_β emission line, whereas the apparent Eddington ratios were computed using the 15–150 keV luminosities.

addition to PBC J1540.3+1415-1 and PBC J1540.3+1415-2 that were discussed in the previous section, the counterpart of PBC J0116.3+3102 (also known as NGC 452) also makes a pair with NGC 444 around 131.8 kpc away.

Other examples of galaxy pairs discovered in the present sample are NGC 5100 NED 02 and MCG +09−19−015 NED 02, the optical counterparts of PBC J1321.1+0858 and PBC J1115.3+5425; these two objects are associated with a nearby galaxy with similar redshift that is located at 23.7 kpc and 113.7 kpc distance, respectively. The AGNs associated with PBC J0223.4+4549 belong instead to a triple system (VZW232) according to NED, although no redshift is available for the other two members of the group. Finally, the active galaxy associated with PBC J1254.8−2655 belongs to a group of objects and more specifically is listed as AM 1252−264 in the catalogue of southern peculiar galaxies and associations assembled by Arp & Madore (1987); interestingly, another member of this group, 2MASX J12544294−2657107, is also visible in X-rays, but is softer and less luminous than the BAT counterpart. We also have a few cases where the galaxy associated with the high-energy source seems to interact with a nearby companion; one such clear case is that of the counterpart of PBC J2035.2+2604.

Overall, we estimate that the fraction of AGNs in the present sample that display evidence of interaction or clustering is around 20%, which is a value very close to that found by Koss et al. (2010) in a more accurate analysis of a set of known active galaxies detected by BAT. This high rate of apparent mergers suggests that AGN activity and merging are critically linked for the moderate-luminosity AGNs in the BAT sample. We also note that a few sources display the properties of radio-loud AGN: at least four (the counterparts of PBC J0459.8+2705, PBC J0602.5+6522, PBC J0654.5+0703, and PBC J1540.3+1415 (specifically object N.3)) display strong radio emission and are characterized by a flat spectrum at these frequencies; their radio morphology is that of a compact source. Two remaining objects are clearly radio galaxies. PBC J0709.2−3601, also known as PKS 0707−35, is a complex and extended source, an edge-brightened double, with two compact outer components of which the south-east one is stronger; two weaker inner components extend away from the axis that joins the outer components and give a slight twist to the structure (Jones & McAdam 1992). PBC J0950.0+7315, also named 4C 73.08, is also a giant double-lobed radio-galaxy, with 13 arcmin angular size between hotspots and a clear FRII morphology (Aretxaga et al. 2001; Hardcastle & Worrall 1999).

We conclude that around 9% of the AGNs in the present sample are radio loud. This percentage is close to what is generally observed among active galaxies. Moreover, we note that the black hole masses listed in Table 6 cover quite a wide range from a few 10^6 to around 7×10^8 $M_\odot$; the Eddington ratio also spans from 0.001 to 0.2, suggesting that BAT AGNs tend to cover a broad range in the parameter space.

Finally, even if this matter is beyond the scope of this paper because it would need a more careful selection of the sample of sources, we checked possible correlations between optical emission line fluxes (H_α, H_β and OIII) and hard X-ray flux (15–150 keV). Using the least-squares bisector method (Isobe et al. 1986), we found no evident correlation between the above

optical quantities and the 15–150 keV hard X-ray flux, obtaining correlation coefficients $R^2 < 0.15$, as previously suggested by Winter et al. (2010). We do not expect a correlation between line strength and source class, because the latter is defined through the ratio of lines and through their width, and not through their strength. Moreover, to the best of our knowledge, there is no known correlation between line strength and redshift, because AGNs are not standard candles; also, the fact that almost all sources in our sample lie at low z (<0.2) does not grant a wide enough baseline for the redshift range to properly explore this point.

6. Conclusions

We have either provided for the first time or confirmed or corrected the optical spectroscopic identifications of 73 sources belonging to the Palermo 54-month *Swift*/BAT catalogue (Cusumano et al. 2010).

This was achieved by performing a multisite observational campaign in Europe and Central and South America. Only for PBC J1540.3+1415 we found more than one optical counterpart, specifically, three objects that most likely emit at high energies.

We found that our sample is dominated by extragalactic objects with only six sources of galactic nature. The extragalactic sample is composed of 69 AGNs (35 of type 1, 33 of type 2, and 1 QSO), with redshifts between 0.006 and 1.137. Among them we highlighted some peculiar objects, such as two galaxies displaying LINER features, one starburst galaxy, two XBONGs, three transition objects, and one object with the properties of an NLS1. For 29 type 1 AGNs we estimated the BLR size, velocity, and the central black-hole mass as well as their Eddington ratio. The AGNs sample presented in this work shows a large portion (around 20%) of objects that display evidence of interaction or clustering, while only 9% show indications of being radio loud.

For the six galactic sources we found two that are most likely magnetic CVs belonging to the IP subclass, three objects with a tentative IP classification, and only one source with non-magnetic properties. Finally, we determined possible correlations between optical emission line fluxes (H_α, H_β and OIII) and hard X-ray flux (15–150 keV), as well as correlations for source class or redshift, but no evident correlation was found.

These results point out the efficiency of using catalogue cross-correlation and/or follow-up X-ray observations from satellites such as *Chandra*, ROSAT, or *Swift* that are capable of providing arcsec-sized error boxes followed by optical spectroscopy to determine the actual nature of still unidentified BAT sources.

Acknowledgements. We thank John Stephen for the useful comments and suggestions, Silvia Galleti for Service Mode observations at the Loiano Telescope, and Roberto Gualandi for night assistance, Giorgio Martorana for Service Mode observations at the Asiago Telescope and Luciano Traverso for coordinating them, Manuel Hernández, Rodrigo Hernández and Josè Velasquez for Service Mode observations at the CTIO telescope, and Fred Walter for coordinating them. We also acknowledge the use of public data from the *Swift* data archive. This research has made use of the ASI Science Data Center Multimission Archive, of the NASA Astrophysics Data System Abstract Service, the NASA/IPAC Extragalactic Database (NED), of the NASA/IPAC Infrared Science Archive, which are operated by the Jet Propulsion Laboratory, California Institute of Technology, under contract with the National Aeronautics and Space Administration and of data obtained from the High Energy Astrophysics Science Archive Research Center (HEASARC), provided by NASA's GSFC. This publication made use of data products from the Two Micron All Sky Survey (2MASS), which is a joint project of the University of Massachusetts and the Infrared Processing and Analysis Center/California Institute of Technology, funded by the National Aeronautics and Space Administration and the National Science Foundation. This research has also made use of data extracted from the 6dF Galaxy Survey and the Sloan Digitized Sky Survey archives; the SIMBAD database operated at the CDS, Strasbourg, France, and of the HyperLeda catalogue operated at the Observatoire de Lyon, France. The authors acknowledge the ASI and INAF financial support via grants Nos. I/033/10/0, I/009/10/0; P.P. is supported by the INTEGRAL ASI-INAF grant No. I/033/10/0. L.M. is supported by the University of Padua through grant No. CPDR061795/06. G.G. is supported by FONDECYT 1085267. V.C. is supported by the CONACyT research grants 54480 and 151494 (Mexico). D.M. is supported by the Basal CATA PFB 06/09, and FONDAP Center for Astrophysics grant No. 15010003.

References

Aretxaga, I., Terlevich, E., Terlevich, R. J., et al. 2001, MNRAS, 325, 636
Arp, H. C., & Madore, B. 1987 (Cambridge, New York: Cambridge University Press)
Barthelmy, S. D. 2004, Proc. SPIE, 5165, 175
Baumgartner, W. H., Tueller, J., Markwardt C. B., et al. 2013, ApJS, 207, 19
Burrows, D. N., Hill, J. E., Nousek, J. A., et al. 2004, Proc. SPIE, 5165, 201
Cardelli, J. A., Clayton, G. C., & Mathis, J. S. 1989, ApJ, 345, 245
Comastri, A., Mignoli, M., Ciliegi, P., et al. 2002, ApJ, 571, 771
Cusumano, G., La Parola, V., Segreto, A., et al. 2010, A&A, 524, A64
Gehrels, N., Chincarini, G., Giommi, P., et al. 2004, ApJ, 611, 1005
Halpern, J. P. 2013, ATel, #5208
Hardcastle, M. J., & Worrall, D. M. 1999, MNRAS, 309, 969
Heckman, T. M. 1980, A&A, 87, 152
Hill, J. E., Burrows, D. N., Nousek, J. A., et al. 2004, Proc. SPIE, 5165, 217
Ho, L. C. 2008, ARA&A, 46, 475
Ho, L. C., Filippenko, A. V., & Sargent, W. L. W. 1993, ApJ, 417, 63
Ho, L. C., Filippenko, A. V., & Sargent, W. L. W. 1997, ApJS, 112, 315
Horne, K. 1986, PASP, 98, 609
Isobe, T., Feigelson, E. D., & Nelson, P. I. 1986, ApJ, 306, 490
Jones, P. A., & McAdam, W. B. 1992, ApJS, 80, 137
Kaspi, S., Smith, P. S., Netzer, H., et al. 2000, ApJ, 533, 631
Kauffmann, G., Heckman, T. M., Tremonti, C., et al. 2003, MNRAS, 346, 1055
Koss, M., Mushotzky, R., Veilleux, S., et al. 2010, ApJ, 716, 125
Landi, R., Masetti, N., Morelli, L., et al. 2007, ApJ, 669, 109
Masetti, N., Palazzi, E., Bassani, L., et al. 2004, A&A, 426, L41
Masetti, N., Mason, E., Bassani, L., et al. 2006a, A&A, 448, 547
Masetti, N., Pretorius, M. L., Palazzi, E., et al. 2006b, A&A, 449, 1139
Masetti, N., Bassani, L., Bazzano, A., et al. 2006c, A&A, 455, 11
Masetti, N., Morelli, L., Palazzi, E., et al. 2006d, A&A, 459, 21
Masetti, N., Mason, E., Morelli, L., et al. 2008, A&A, 482, 113
Masetti, N., Parisi, P., Palazzi, E., et al. 2009, A&A, 495, 121
Masetti, N., Parisi, P., Palazzi, E., et al. 2010, A&A, 519, A96
Masetti, N., Parisi, P., Jiménez-Bailón, E., et al. 2012, A&A, 538, A123
Masetti, N., Parisi, P., Palazzi, E., et al. 2013, A&A, 556, A120
Monet, D. G., Levine, S. E., Canzian, B., et al. 2003, AJ, 125, 984
Morelli, L. Calvi, V., Masetti, N., et al. 2013, A&A, 556, A135
Osterbrock, D. E. 1989, Astrophysics of Gaseous Nebulae and Active Galactic Nuclei (Mill Valley: Univ. Science Books)
Osterbrock, D. E., & Pogge, R. W. 1985, ApJ, 297, 166
Panessa, F., de Rosa, A., Bassani, L., et al. 2011, MNRAS, 417, 2426
Parisi, P., Masetti, N., Jiménez-Bailón, E., et al. 2009, A&A, 507, 1345
Parisi, P., Masetti, N., Jiménez-Bailón, E., et al. 2012, A&A, 545, A101
Schlegel, D. J., Finkbeiner, D. P., & Davis, M. 1998, ApJ, 500, 525
Skrutskie, M. F., Cutri, R. M., Stiening, R., et al. 2006, AJ, 131, 1163
Stephen, J. B., Bassani, L., Malizia, A., et al. 2006, A&A, 445, 869
Tomsick, J. A., Bodaghee, A., Chaty, S., et al. 2012, ApJ, 754, 145
Ubertini, P., Lebrun, F., Di Cocco, G., et al. 2003, A&A, 411, L131
Veilleux, S., & Osterbrock, D. E. 1987, ApJS, 63, 295
Véron-Cetty, M. P., & Véron, P. 2010, A&A, 518, A10
Vestergaard, M. 2004, Proc. AGN Physics with the Sloan Digital Sky Survey, eds. G. T. Richards, & P. B. Hall, ASP Conf. Ser. (San Francisco: ASP), 311, 69
Voges, W., Aschenbach, B., Boller, T., et al. 1999, A&A, 349, 389
Warner, B. 1995, Cataclysmic variable stars (Cambridge: Cambridge University Press)
Winkler, H. 1992, MNRAS, 257, 677
Winkler, C., Courvoisier, T. J.-L., Di Cocco, G., et al. 2003, A&A, 411, L1
Winter, L., Lewis, K. T., Koss, M., et al. 2010, ApJ, 710, 503
Wright, E. L. 2006, PASP, 118, 1711
Wu, X.-B., Wang, R., Kong, M. Z., Liu, F. K., & Han, J. L. 2004, A&A, 424, 793

Pages 10 to 17 are available in the electronic edition of the journal at http://www.aanda.org

Table 2. Main results obtained from the analysis of the optical spectra of the 35 type 1 AGNs.

Object	$F_{H_\alpha}{}^*$	F_{H_β}	$F_{[OIII]}$	Class	z	D_L	$E(B-V)$		2MASS name
						(Mpc)	Gal.	AGN	
PBC J0000.9−0708	16.2 ± 2.8 [25.4 ± 5.7]	1.67 ± 0.53 [3.59 ± 0.45]	26.3 ± 2.1 [31.5 ± 2.3]	Sy1.9	0.038	167.5	0.034	0.869	2MASX J00004876−0709117
PBC J0050.8+7648	129 ± 8.3 [297 ± 31.7]	28.8 ± 5.2 [96.1 ± 16.9]	12.8 ± 1.5 [41.1 ± 4.1]	Sy1.2	0.128	600.1	0.435	0.074	2MASS J00510664+7650359
PBC J0116.3+3102	84.1 ± 51.8 [98.2 ± 59.7]	abs. [abs.]	18.6 ± 4.4 [23.1 ± 4.8]	Sy1.9	0.018	78.2	0.070	–	2MASS J01161480+3102017
PBC J0149.3−5017	125 ± 17 [134.0 ± 16.5]	34.1 ± 6.3 [37.1 ± 8.2]	16.0 ± 1.3 [17.4 ± 2.1]	Sy1.2	0.0299	131.0	0.022	0.224	2MASX J01492228-5015073
PBC J0157.3+4715	378 ± 49 [563 ± 68]	36.9 ± 10.1 [80.4 ± 13.9]	11.3 ± 2.3 [18.5 ± 3.2]	Sy1.2	0.049	217.7	0.165	0.859	2MASX J01571097+4715588
PBC J0311.9+5029	85.9 ± 10.1 [442 ± 44]	11.2 ± 3.5 [158 ± 36]	19.3 ± 1.7 [183 ± 16]	Sy1.5	0.062	278.0	0.759	0	2MASX J03120291+5029147
PBC J0429.7−6703	212 ± 18 [234 ± 19]	53.1 ± 7.6 [59.1 ± 10.2]	30.9 ± 3.2 [34.5 ± 3.8]	Sy1.5	0.065	292.1	0.044	0.312	2MASX J04294735−6703205
PBC J0440.8+2739	89.2 ± 10.8 [497 ± 65]	5.6 ± 1.7 [65.9 ± 19.5]	9.3 ± 0.9 [102 ± 12]	Sy1.5	0.038	167.5	0.805	0.931	2MASX J04404770+2739466
PBC J0532.7+1346	33.5 ± 7.8 [224 ± 40]	< 0.4 [<4.1]	1.3 ± 0.5 [17.5 ± 5.7]	Sy1.5	0.024	104.7	0.843	>2.831	2MASX J05325752+1345092
PBC J0535.6+4011	133 ± 13 [551 ± 47]	20.1 ± 5.3 [162 ± 30]	31.4 ± 2.4 [198 ± 13]	Sy1.5	0.021	91.4	0.635	0.166	2MASX J05353211+4011152
PBC J0543.9−4325	5.4 ± 0.8 [10.5 ± 1.7]	1.4 ± 0.4 [2.4 ± 0.8]	4.8 ± 0.5 [10.8 ± 1.4]	Sy1.8	0.045	199.3	0.051	0.408	2MASX J05440009−4325265
PBC J0602.5+6522	460 ± 251 [597 ± 324]	<0.3 [<1.1]	44.5 ± 5.8 [62.5 ± 8.1]	Sy1.9	0.017	73.8	0.108	>5.035	2MASX J06023793+6522161
PBC J0609.4−6243	87.6 ± 14.1 [99.4 ± 15.1]	8.5 ± 1.7 [9.1 ± 1.8]	4.9 ± 1.2 [6.8 ± 1.4]	Sy1.5	0.157	749.7	0.053	1.286	2MASX J06100652−6243125
PBC J0635.0−7441	297 ± 28 [369 ± 41]	70.3 ± 14.2 [111 ± 20]	12.7 ± 4.5 [17.9 ± 3.6]	Sy1	0.112	519.7	0.106	0.144	2MASS J06340353−7446377
PBC J0654.5+0703	317 ± 34 [590 ± 49]	22.8 ± 5.5 [62.1 ± 13.1]	12.6 ± 1.9 [137 ± 6.8]	Sy1.5	0.024	104.7	0.295	1.152	2MASS J06543417+0703210
PBC J0749.2−8634	153 ± 14 [220 ± 21]	25.3 ± 4.6 [39.2 ± 6.7]	10.1 ± 1.9 [16.2 ± 3.2]	Sy1.2	0.109	504.7	0.180	0.647	2MASX J07504720−8632118
PBC J0803.4+0840	215 ± 34 [217 ± 40]	12.1 ± 3.9 [14.6 ± 5.1]	93.7 ± 3.9 [98.2 ± 5.2]	Sy1.5	0.047	208.5	0.022	1.582	2MASX J08032736+0841523
PBC J0818.5−1420	44.1 ± 7.3 [47.5 ± 8.2]	16.1 ± 2.7 [16.2 ± 2.8]	10.1 ± 1.1 [12.3 ± 1.4]	Sy1.5	0.107	494.8	0.074	0.024	2MASS J08182026−1425527
PBC J0917.2−6454	49.8 ± 6.9 [85.3 ± 11.4]	8.3 ± 2.2 [16.6 ± 4.1]	71.4 ± 5.1 [132 ± 10.7]	Sy1.9	0.086	393.1	0.224	0.562	2MASS J09172721−6456270
PBC J0942.1+2342	55.1 ± 17.3 [81.1 ± 19.1]	48.1 ± 0.4 [70.8 ± 23.5]	37.1 ± 4.5 [37.4 ± 4.6]	Sy1.5	0.022	95.8	0.027	0	2MASX J09420476+2341066
PBC J1002.3+0304	62.8 ± 9.8 [76.5 ± 10.4]	5.8 ± 02.7 [8.1 ± 3.1]	39.1 ± 6.7 [51.7 ± 7.1]	Sy1.8/1.9	0.023	100.2	0.082	1.147	2MASX J10020701+0303277
PBC J1020.5−0235	94.4 ± 32.1 [94.5 ± 32.4]	76.3 ± 30.2 [76.4 ± 30.9]	6.4 ± 2.5 [7.1 ± 2.6]	Sy1	0.060	268.7	0.044	0	2MASX J10195855−0234363
PBC J1254.8−2655	523 ± 65 [660 ± 77]	72.2 ± 22.6 [98.9 ± 30.7]	72.3 ± 4.9 [94.6 ± 6.9]	Sy1.5	0.060	268.7	0.081	0.813	2MASX J12545637−2657021
PBC J1349.0+4443	22.6 ± 4.4 [22.6 ± 4.4]	17.5 ± 6.4 [23.1 ± 7.3]	7.3 ± 1.1 [8.1 ± 1.4]	Sy1.2	0.065	292.1	0.015	0	2MASX J13490841+4441295

Notes. Emission line fluxes are reported both as observed and (between square brackets) corrected for the intervening Galactic absorption $E(B-V)_{Gal}$ along the object line of sight (from Schlegel et al. 1998). Line fluxes are in units of 10^{-15} erg cm^{-2} s^{-1}, The typical error on the redshift measurement is ±0.001; $^{(*)}$ blended with [N II] lines.

Table 2. continued.

Object	F_{H_α} *	F_{H_β}	$F_{[OIII]}$	Class	z	D_L	$E(B-V)$		2MASS name
						(Mpc)	Gal.	AGN	
PBC J1416.8−1158	132 ± 31 [416 ± 72]	55.5 ± 11.1 [75.1 ± 15.1]	33.7 ± 2.4 [41.2 ± 2.9]	Sy1.5	0.099	455.4	0.072	0.634	2MASX J14165001−1158577
PBC J1540.3+1415–3	146 ± 15 [168 ± 18]	34.1 ± 7.5 [36.3 ± 7.9]	12.2 ± 1.1 [14.1 ± 1.6]	Sy1.2	0.12	559.7	0.052	0.522	2MASS J15400784+1411371
PBC J1824.2+1846	80.1 ± 11.7 [116 ± 17]	9.6 ± 2.6 [18.1 ± 4.9]	90.9 ± 5.1 [174 ± 9.8]	Sy1.9	0.067	301.5	0.223	0.774	2MASX J18241083+1846088
PBC J1846.0+5607	20.9 ± 2.7 [23.4 ± 3.1]	2.1 ± 0.6 [3.1 ± 0.9]	7.9 ± 0.5 [9.4 ± 0.6]	Sy1.5	0.07	315.7	0.058	0.931	2MASS J18455688+5610022
PBC J1926.6+4131	31.1 ± 24.2 [33.4 ± 25.9]	<0.8 [<0.9]	<0.8 [<1.3]	Sy1.9	0.072	325.1	0.112	>2.46	2MASX J19263018+4133053
PBC J2035.2+2604	258 ± 18 [476 ± 33]	28.2 ± 7.9 [69.8 ± 19.6]	76.5 ± 4.5 [179 ± 10.5]	NLS1	0.05	222.3	0.283	0.834	2MASX J20350566+2603301
PBC J2116.2+2519	83.4 ± 12.8 [102 ± 16]	23.7 ± 2.6 [34.8 ± 3.8]	5.4 ± 0.6 [7.6 ± 0.8]	Sy1.2	0.153	728.8	0.130	0.023	2MASX J21161028+2517010
PBC J2123.9+3407	149 ± 20 [202 ± 27]	18.3 ± 5.1 [27.2 ± 7.6]	18.8 ± 1.1 [28.7 ± 1.7]	Sy1.5	0.083	377.7	0.144	0.916	2MASX J21240027+3409114
PBC J2157.4−0611	3570 ± 772 [3690 ± 798]	394 ± 94.9 [426 ± 103]	305 ± 34.2 [329 ± 36.9]	Sy1.5	0.176	850.2	0.03	1.064	2MASS J21572678−0610176
PBC J2248.8+1725	15.2 ± 3.9 [17.7 ± 4.5]	1.3 ± 0.5 [1.7 ± 0.7]	8.9 ± 0.8 [10.8 ± 0.9]	Sy1.8	0.086	392.1	0.083	1.24	2MASS J21572678−0610176
PBC J2307.9+4015	441 ± 93.8 [558 ± 118]	27.1 ± 9.7 [36.1 ± 12.9]	23.7 ± 2.1 [34.1 ± 3.1]	Sy1.5	0.073	329.9	0.122	1.619	2MASX J23075724+4016393

Table 3. Main results obtained from the analysis of the optical spectra of the 33 type 2 AGNs.

Object	F_{H_α} *	F_{H_β}	$F_{[OIII]}$	Class	z	D_L	$E(B-V)$		2MASS name
						(Mpc)	Gal.	AGN	
PBC J0034.6−0424	–	1.44 ± 0.31 [1.61 ± 0.37]	17.0 ± 0.4 [18.7 ± 1.1]	Sy 2	0.213	1051.6	0.039	–	2MASX J00343284−0424117
PBC J0038.5+2336	3.65 ± 1.18 [3.84 ± 2.41]	abs. [abs.]	9.31 ± 1.09 [9.23 ± 2.37]	Sy 2	0.025	109.1	0.028	–	2MASX J00383214+2336475
PBC J0128.6−6038	98.2 ± 45.4 [128.0 ± 46.5]	14.2 ± 3.7 [21.4 ± 6.9]	83.5 ± 25.2 [92.9 ± 21.1]	Sy 2	0.203	996.5	0.024	1.056	2MASX J01290761−6038423
PBC J0223.4+4549	59.8 ± 11.2 [76.2 ± 29.2]	6.9 ± 2.8 [9.4 ± 2.8]	107 ± 7 [147 ± 10]	Sy 2	0.062	278.0	0.112	1.001	2MASX J02233309+4549162
PBC J0238.3−6116	12.4 ± 2.4 [12.5 ± 2.5]	abs. [abs.]	7.3 ± 0.8 [7.9 ± 1.1]	Sy 2	0.054	240.8	0.024	–	2MASX J02384313−6117227
PBC J0243.9+5323	4.5 ± 1.1 [10.8 ± 2.1]	abs. [abs.]	1.6 ± 0.3 [5.9 ± 1.2]	Likely Sy 2	0.036	158.4	0.409	–	2MASX J02440296+5328281
PBC J0359.0−3017	16.5 ± 4.5 [32.7 ± 4.7]	4.2 ± 0.7 [4.3 ± 0.6]	18.4 ± 1.5 [19.5 ± 1.5]	Sy 2	0.094	430.9	0.01	0.93	2MASX J03590885−3018102
PBC J0459.8+2705	37.2 ± 3.9 [448 ± 64]	1.8 ± 0.6 [54.5 ± 13.3]	16.1 ± 1.3 [484 ± 34]	Sy 2	0.061	273.3	1.212	1.013	2MASX J04595608+2706024
PBC J0515.3+1856	42.5 ± 3.4 [168 ± 16]	1.5 ± 0.4 [9.9 ± 4.5]	31.9 ± 2.7 [217 ± 16]	Sy 2	0.023	100.2	0.606	1.714	2MASX J05151978+1854515
PBC J0709.2−3601	5.5 ± 0.7 [25.3 ± 3.8]	<0.9 [<3.9]	3.9 ± 0.9 [31.7 ± 3.1]	Sy 2	0.110	509.7	0.745	>0.786	2MASS J07091409−3601219

Notes. Emission line fluxes are reported both as observed and (between square brackets) corrected for the intervening Galactic absorption $E(B-V)_{Gal}$ along the object line of sight (from Schlegel et al. 1998). Line fluxes are in units of 10^{-15} erg cm^{-2} s^{-1}, The typical error on the redshift measurement is ±0.001; (*) blended with [N II] lines.

Table 3. continued.

Object	F_{H_α} *	F_{H_β}	$F_{[OIII]}$	Class	z	D_L	$E(B-V)$		2MASS name
						(Mpc)	Gal.	AGN	
PBC J0747.7−7326	0.5 ± 0.1 [7.4 ± 1.4]	abs. [abs.]	8.2 ± 1.2 [32.4 ± 4.7]	LINER	0.036	158.4	0.440	–	2MASX J07473839−7325533
PBC J0855.8−2855	3.4 ± 0.3 [4.6 ± 0.4]	<0.9 [<1.4]	<0.3 [<0.4]	Likely Sy 2	0.073	329.9	0.150	>0.133	2MASX J08551746−2854218
PBC J0859.5+4457	88.9 ± 8.8 [90.9 ± 24.9]	11.4 ± 3.1 [12.1 ± 3.3]	10.6 ± 3.3 [12.5 ± 4.2]	Trans. obj	0.006	26.2	0.022	0.927	2MASX J08593045+4454504
PBC J0929.6+6231	5.3 ± 2.2 [5.9 ± 2.3]	–	8.1 ± 1.1 [8.9 ± 1.2]	Sy 2	0.025	109.1	0.033	–	2MASX J09293791+6232382
PBC J0950.0+7315	13.4 ± 3.6 [14.5 ± 3.7]	1.6 ± 0.5 [1.8 ± 0.6]	26.9 ± 3.7 [29.2 ± 3.9]	Sy 2	0.058	259.3	0.027	0.993	2MASX J09494596+7314232
PBC J1017.2−0404	12.4 ± 1.6 [14.1 ± 4.3]	1.3 ± 1.2 [1.3 ± 1.2]	9.8 ± 1.3 [11.4 ± 1.3]	Sy 2	0.041	181.1	0.047	1.279	2MASX J10171680−0404558
PBC J1034.2+7301	8.4 ± 3.1 [17.4 ± 4.4]	abs. [abs.]	7.6 ± 3.9 [11.2 ± 5.6]	XBONG/ Likely Sy 2	0.022	95.8	0.128	–	2MASX J10342366+7300499
PBC J1113.6+7942	13.6 ± 3.1 [13.9 ± 3.6]	<1.1 [<1.3]	23.4 ± 3.1 [26.9 ± 3.1]	Sy 2	0.037	162.9	0.046	>1.266	2MASX J11144385+7943357
PBC J1115.3+5425	16.8 ± 1.2 [16.8 ± 1.3]	1.9 ± 0.6 [1.9 ± 0.6]	28.1 ± 1.4 [28.9 ± 1.5]	Sy 2	0.071	320.4	0.014	1.083	2MASX J11151992+5423167
PBC J1145.4+5858	abs. [abs.]	<1.8 [<1.9]	abs. [abs.]	Type 2	0.008	34.5	0.022	–	2MASX J11453317+5858408
PBC J1231.4+5759	211 ± 20 [217 ± 21]	32.3 ± 3.7 [33.6 ± 3.9]	78.6 ± 4.8 [83.1 ± 4.9]	starburst galaxy	0.011	47.5	0.013	0.782	2MASX J12312214+5757528
PBC J1240.8+2736	35.4 ± 5.7 [36.6 ± 6.1]	1.1 ± 0.5 [1.1 ± 0.5]	5.6 ± 1.1 [5.9 ± 1.2]	Sy 2	0.056	250	0.017	2.338	2MASX J12404640+2733535
PBC J1321.1+0858	60.1 ± 4.2 [63.8 ± 4.2]	9.9 ± 3.9 [11.5 ± 4.3]	12.6 ± 3.1 [12.7 ± 3.2]	LINER	0.033	144.9	0.031	0.636	2MASX J13205961+0858421
PBC J1355.5+3523	–	–	–	XBONG	0.100	460.3	0.016	–	2MASX J13553383+3520573
PBC J1540.3+1415–1	20.9 ± 1.6 [23.5 ± 1.8]	7.2 ± 0.9 [8.4 ± 1.1]	58.7 ± 1.3 [68.1 ± 1.4]	Trans. obj.	0.0508	225.5	0.049	0	2MASX J15401296+1416432
PBC J1540.3+1415–2	8.1 ± 0.5 [9.1 ± 0.6]	2.3 ± 0.3 [2.8 ± 0.3]	2.1 ± 0.3 [2.5 ± 0.3]	Trans. obj.	0.05	222.3	0.049	0.123	2MASX J15401234+1416592
PBC J1821.2+5957	24.9 ± 4.1 [9.1 ± 0.6]	3.5 ± 1.4 [2.8 ± 0.3]	36.7 ± 2.3 [2.5 ± 0.3]	Sy2	0.099	455.4	0.045	0.772	2MASX J18212680+5955209
PBC J1826.6+3251	17.4 ± 3.5 [21.1 ± 4.2]	<1.5 [<2.9]	31.7 ± 2.1 [45.2 ± 2.9]	Sy2	0.022	95.8	0.115	>0.896	2MASX J18263239+3251300
PBC J1903.7+3349	35.7 ± 11.2 [44.9 ± 14.1]	4.8 ± 1.5 [6.1 ± 1.9]	60.4 ± 3.2 [82.1 ± 4.3]	Sy2	0.015	65	0.096	0.907	2MASX J19034916+3350407
PBC J2010.2+4759	2.2 ± 0.4 [5.9 ± 1.1]	abs. [abs.]	1.4 ± 0.2 [5.6 ± 0.8]	Sy2	0.026	113.6	0.453	–	2MASX J20101740+4800214
PBC J2150.7+1405	41.6 ± 6.6 [59.7 ± 9.5]	5.3 ± 0.7 [8.1 ± 1.1]	16.1 ± 2.5 [26.5 ± 4.1]	Sy2	0.031	135.9	0.141	0.909	2MASX J21504675+1406369
PBC J2307.8+2244	9.3 ± 6.6 [16.7 ± 11.8]	1.3 ± 0.1 [2.7 ± 0.2]	29.8 ± 2.2 [69.1 ± 5.1]	Sy2	0.035	153.9	0.269	0.740	2MASX J23074887+2242367
PBC J2343.8+0539	9.4 ± 2.2 [15.3 ± 3.6]	<1.1 [<3.4]	22.6 ± 2.3 [35.1 ± 3.6]	Sy2	0.056	250	0.137	0.435	2MASX J23435956+0538233

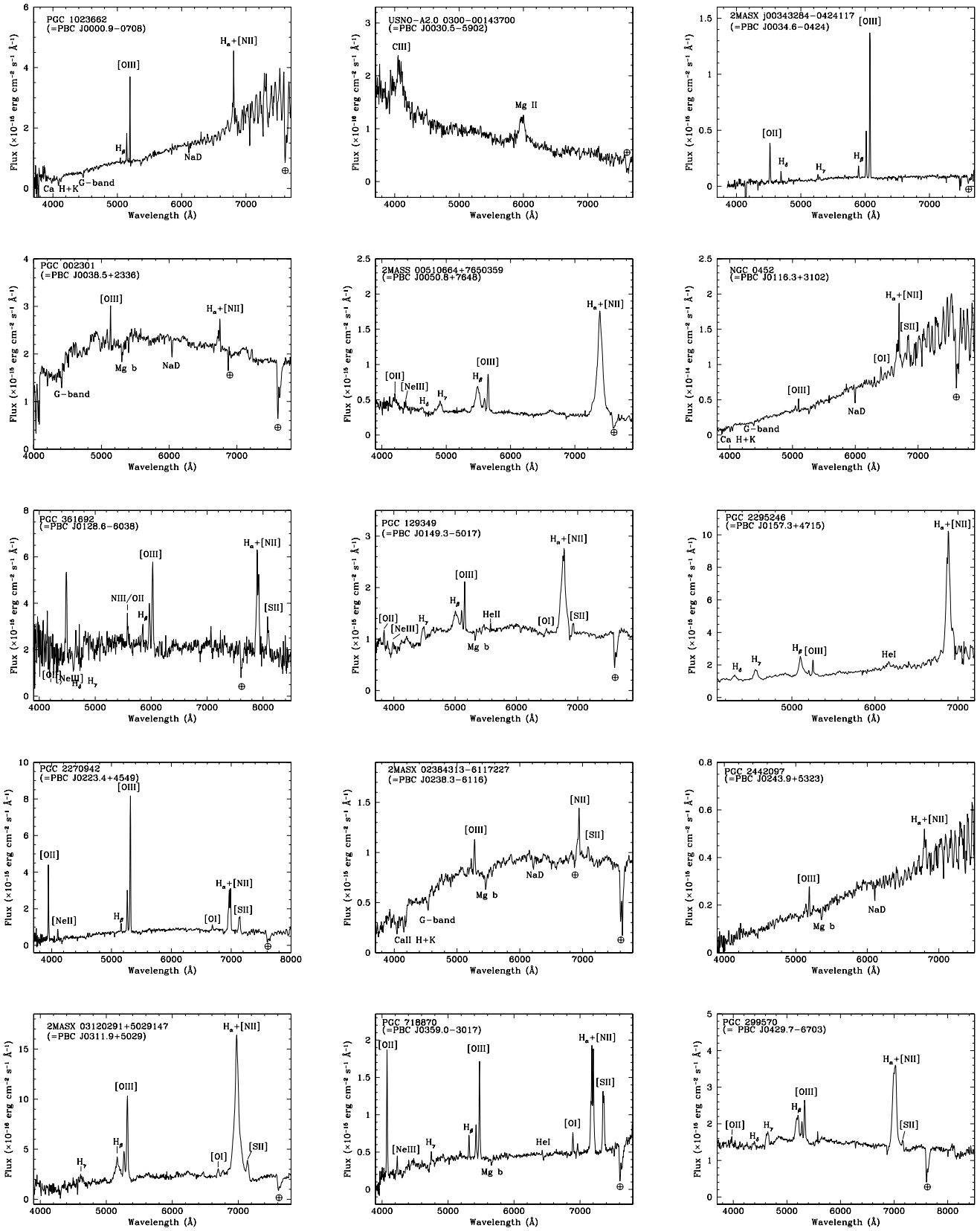

Fig. 2. Spectra of the optical counterpart of AGNs presented in this work (not corrected for the intervening Galactic absorption). For each spectrum the main spectral features are labelled.

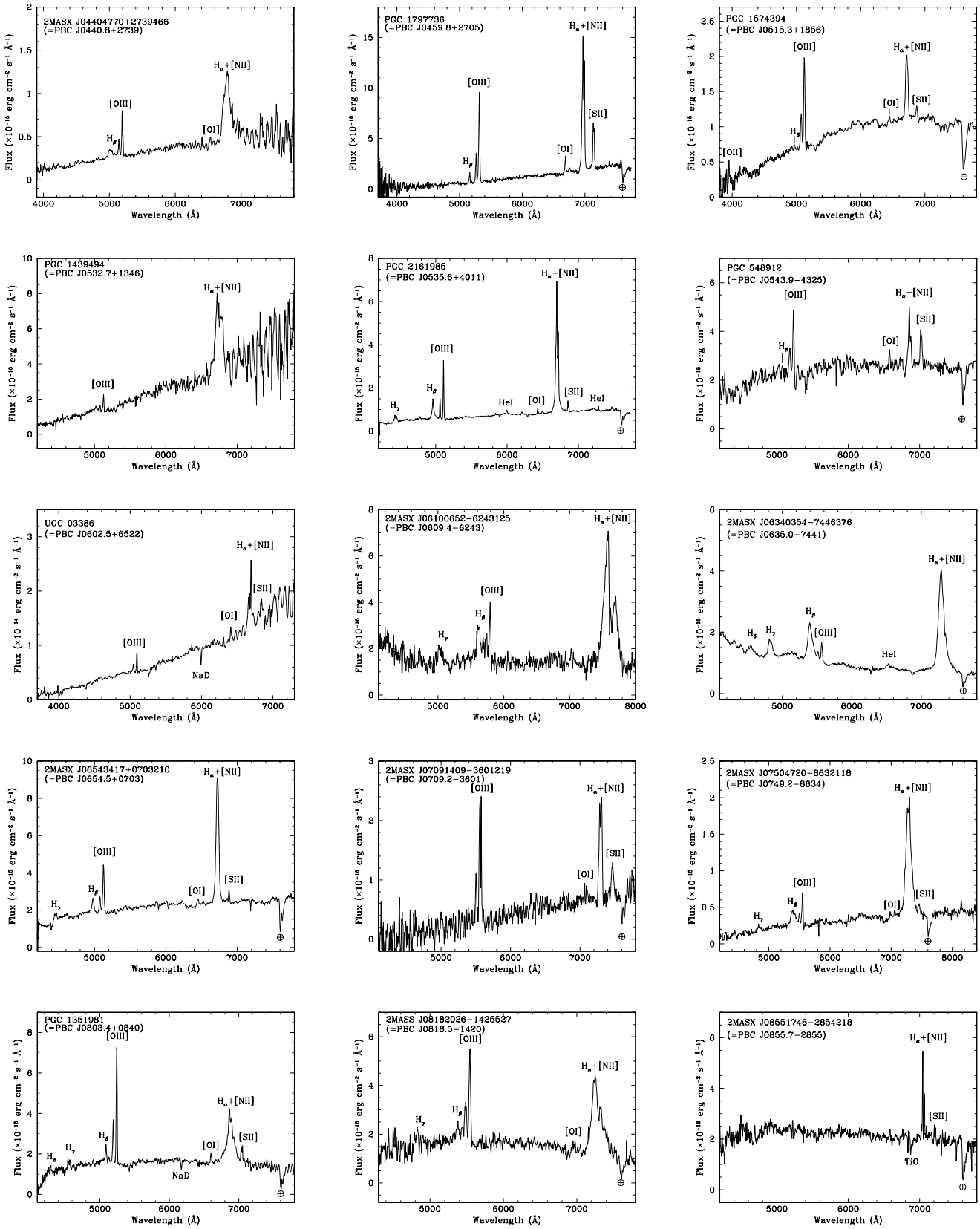

Fig. 2. continued.

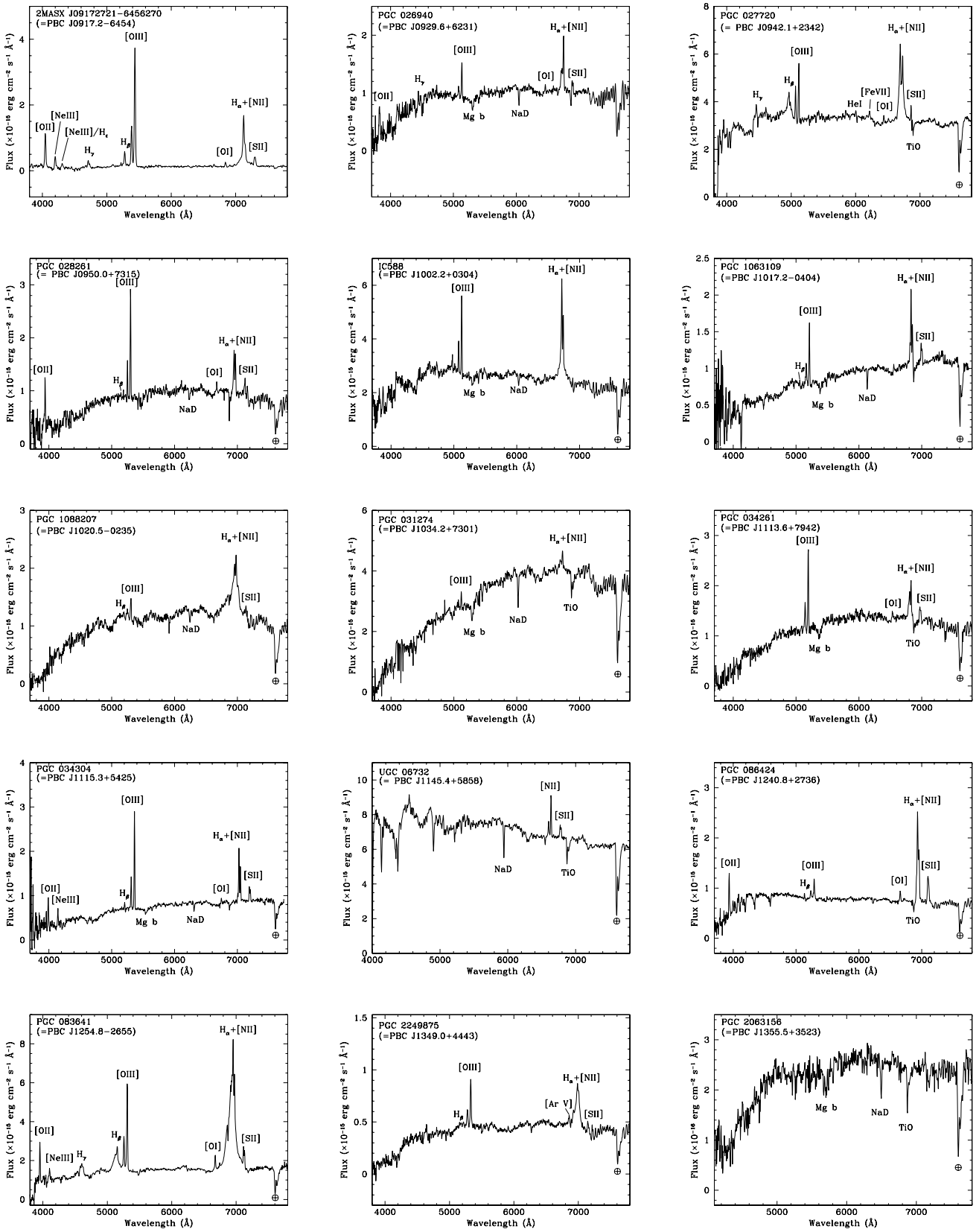

Fig. 2. continued.

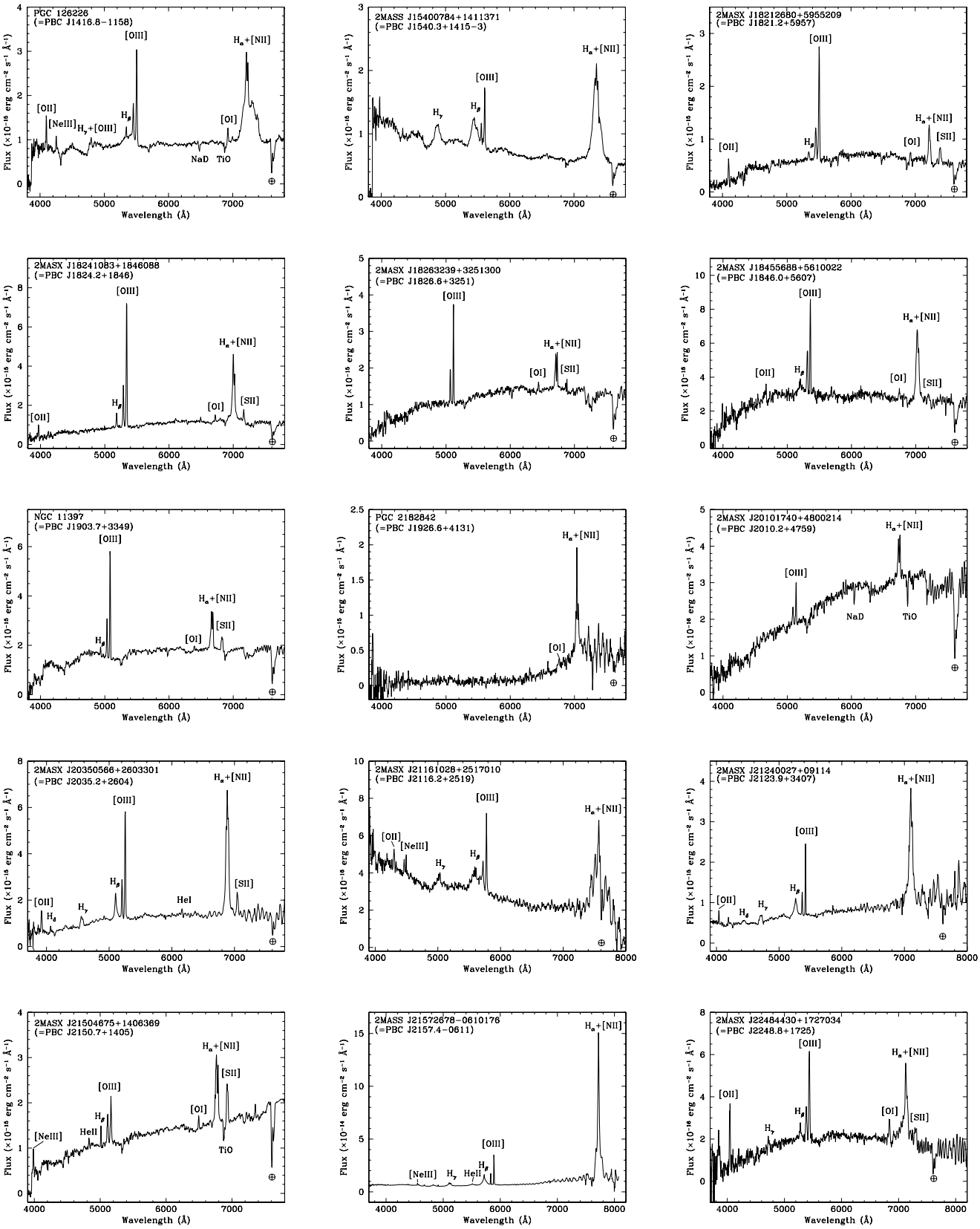

Fig. 2. continued.

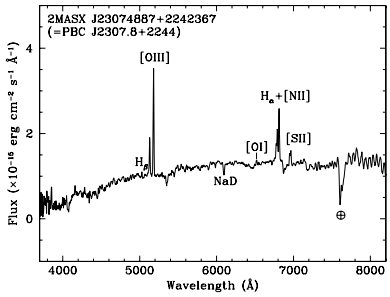

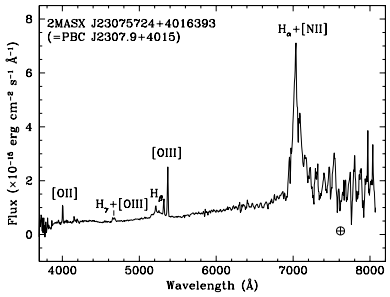

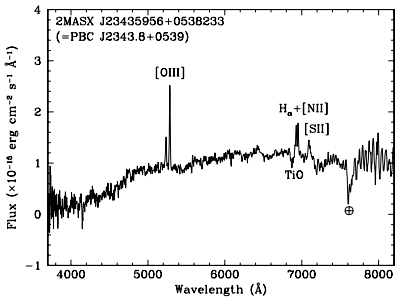

Fig. 2. continued.